

Suppression of AMP kinase activity in skeletal muscle improves metabolic abnormalities of streptozotocin-induced insulin-deficient diabetes mellitus in mice

Shigefumi Yokota

Department of Physiological Science

School of Life Science

Graduate University for Advanced Studies (*SOKENDAI*)

2012

CONTENTS

ABSTRACT	Page 2
INTRODUCTION	Page 4
METHODS	Page 7
RESULTS	Page 12
DISCUSSION	Page 21
ACKNOWLEDGEMENTS	Page 27
REFERENCE	Page 28
FIGURES	Page 33
TABLES	Page 59

ABSTRACT

Type 1 diabetes mellitus (T1DM) is caused by a consequence of pancreatic β -cell destruction leading to insulin deficiency, a defect that causes hyperglycemia, ketoacidosis, high plasma fatty acid level and cachexia. I explored the role of AMPK in skeletal muscle in those metabolic changes in streptozotocin (STZ)-induced insulin-deficient diabetes mellitus (IDDM) mice. I found that STZ-induced IDDM activates AMPK and its signaling pathways in skeletal muscle. Surprisingly, inhibition of AMPK activation in skeletal muscle in STZ-induced IDDM by preferentially expressing dominant-negative AMPK (DN-AMPK), decreased plasma concentration of glucose, fatty acids, ketone bodies, and gluconeogenic hormones, although plasma insulin level remains low. Moreover, STZ-treated DN-AMPK expressing mice improved the weight loss of white adipose tissue (WAT) and skeletal muscle, and body weight loss, leading to increased survival rate. WAT in STZ-induced IDDM mice increased UCP1 (uncoupling protein 1) expression as well as decreased expression of lipogenic enzymes, but those were returned to the control levels in STZ-treated DN-AMPK expressing mice. STZ-treated DN-AMPK expressing mice recovered plasma concentration of leptin that has been known to stimulate whole body glucose and lipid metabolism in IDDM.

Interleukin-6 (IL-6) is released from skeletal muscle and stimulates lipolysis in adipose tissues, and a novel myokine, irisin, induces thermogenic protein UCP1 in WAT. I found that

expressions of IL-6 and irisin increased in skeletal muscle and their plasma concentrations in STZ-induced IDDM mice, but those returned to the control levels in STZ-treated DN-AMPK expressing mice. Furthermore, infusion of neutral antibody for IL-6 or infusion of leptin by osmotic minipump, improved the metabolic changes in STZ-induced IDDM mice, similar to those in STZ-treated DN-AMPK expressing mice. These results thus unveil a key role for muscle AMPK in metabolic abnormalities in STZ-induced IDDM, and important role of organ networks in the metabolic regulation.

INTRODUCTION

Type 1 diabetes mellitus (T1DM) is caused by a consequence of pancreatic β -cell destruction leading to insulin deficiency, a defect that causes hyperglycemia, ketoacidosis, high plasma fatty acid level and cachexia (1, 2). Cachexia includes atrophy of white adipose tissue and skeletal muscle, leading to a deadly condition. At present, insulin is only assumed to reverse this lethal catabolic syndrome. However, even with insulin therapy, patients with T1DM suffer secondary complications such as heart disease, nephropathy and hypertension (3-5). Furthermore, long-term insulin treatment underlies the increased ectopic lipid deposition in non-adipose tissues and incidence of coronary artery disease in more than 90% of the T1DM patients after the age of 55 years (6-8), probably because of the insulin's lipogenic and cholesterogenic actions. Moreover, intensive insulin therapy significantly increases risk for hypoglycemia, an event that is disabling and can even be fatal. Thus, despite the profound diabetes-improving and life-saving effects of insulin therapies, additional T1DM therapies are required.

AMPK (AMP-activated protein kinase) is a serine/threonine kinase activated in response to increasing intracellular (AMP and ADP)/ATP ratio (9, 10). AMPK is a heterotrimeric complex comprising of a catalytic α -subunit and regulatory β - and γ -subunits (9). Activation of AMPK promotes catabolic processes producing ATP such as mitochondrial biogenesis, fatty acid oxidation

and glucose utilization, and it inhibits anabolic pathways consuming ATP such as protein synthesis (9). AMPK has been shown to stimulate fatty acid oxidation via direct phosphorylation (Ser79) of acetyl-CoA carboxylase (ACC) and suppression of its activity. Suppression of ACC activity decreases production of malonyl-CoA, an allosteric inhibitor of carnitine palmitoyltransferase I (CPT1) that transports free fatty acids from cytosol to mitochondrion, leading to fatty acid oxidation (11). AMPK also activates PGC-1 α , a transcription co-factor for mitochondrion-related gene expressions, via nicotinamide phosphoribosyltransferase (NAMPT) and SIRT1 (sirtuin-1: a NAD⁺-dependent deacetylase)-dependent pathway (12-14). Moreover, AMPK inhibits protein synthesis via directly phosphorylating TSC2 (Tuberous sclerosis protein 2) and thereby inhibiting mTOR (mammalian target of rapamaicin) and S6K (p70 S6 kinase) signaling pathway (15, 16). Furthermore, AMPK directly phosphorylates ULK1 (unc-51-like kinase 1), and increases the expression of LC3-II (an executive factor of autophagy) (17-19), inducing autophagy.

In the present study, I explored the role of AMPK in skeletal muscle in metabolic changes in STZ-induced insulin-deficient diabetes mellitus (IDDM) in mice. I speculated that insulin deficiency and decreased glucose utilization in skeletal muscle activates AMPK in the tissue. I found that STZ-induced IDDM activates AMPK and its signaling pathways in skeletal muscle. Surprisingly, inhibition of AMPK activation in skeletal muscle in IDDM by expressing dominant-

negative AMPK (DN-AMPK) in the tissue preferentially improved metabolic changes in STZ-induced IDDM such as hyperglycemia and decreased plasma concentrations of free fatty acids, ketone bodies and gluconeogenic hormones such as epinephrine, norepinephrine and corticosterone, although plasma insulin level remains low. Moreover, STZ-treated DN-AMPK expressing mice increased amount of adipose tissues, skeletal muscle, and body weight, and then increased survival rate. STZ-treated DN-AMPK expressing mice also recovered plasma concentration of leptin that stimulates glucose utilization in muscle (20-22) and reverses the impaired whole body glucose metabolism in STZ-induced IDDM (23, 24). The present study provides a novel insight for important role of organ networks in metabolic regulation in IDDM.

METHODS

Animals

Male C57BL/6J mice (Nihon SLC, Hamamatsu, Japan) and skeletal muscle-specific DN-AMPK expressing mice (DN-AMPK mice) (29) were studied at 10 to 12 weeks of age. DN-AMPK mice were overexpressed mutated $\alpha 1$ catalytic subunit of AMPK, which is changed the residue asparagic acid at 157th to alanine (Asp157Ala), preferentially in skeletal muscle under the control of human α -skeletal actin promoter (29). Asp 157 lies in the conserved DFG (subdomain VII in the protein kinase catalytic subunit) motif, which is essential for Mg^{2+} -ATP binding in protein kinases (29). The animals were housed individually in plastic cages at $24^{\circ} \pm 1^{\circ}C$ with lights on from 06:00 to 18:00 hr, and they were maintained with free access to a laboratory diet (Oriental Yeast, Tokyo, Japan) and water. Mice were manipulated by twice intraperitoneal (i.p.) injections of STZ (200 mg/Kg) (Sigma, Tokyo, Japan) on the 1st and 3rd day (STZ-treated WT mice and STZ-treated DN-AMPK mice). Another groups of mice (WT mice and DN-AMPK mice) were injected vehicle as those in STZ-treated mice. One week after the 2nd injection, glucose tolerance test (GTT), fat loading test and pyruvate tolerance test were performed. Blood was collected from the tail every day, and plasma concentration of glucose was measured with kits (Glucose: Glucose CII-test, Wako, Osaka, Japan). Two weeks after the 2nd injection of STZ, mice were decapitated, and tissues and blood samples were collected at 1:00 PM. All animal experiments were approved by the ethics committee for

animal experiments of the National Institute for Physiological Sciences.

Glucose tolerance, pyruvate tolerance and fat loading tests

After overnight fasting, animals were injected i.p. glucose (2 g/kg) for glucose tolerance test (GTT) and sodium pyruvate (2 g/kg) for pyruvate tolerance test, respectively. Blood was collected from the tail at 0, 30, 60, 90, and 120 min after glucose injection. Plasma concentrations of glucose and insulin were measured with kits (Glucose: Glucose CII-test, Wako; Insulin: Mouse Insulin ELISA KIT (U-type), Shibayagi) (see Table 1).

Fat loading test was performed as described previously (30). After 4 hour fasting, mice were ingested triolein (17 μ l/g, KANTO CHEMICAL CO.,INC, Tokyo, Japan) intragastrically by gavage, and blood was collected from the tail serially at 0, 30, 60, 120, 180 and 300 minutes. Plasma concentrations of free fatty acids, triglyceride and insulin were measured with kits (free fatty acids: NEFA C-test, Wako; triglyceride: Triglyceride E-test, Wako; Mouse Insulin ELISA KIT (U-type), Shibayagi) (see Table 1).

Immunoblot analysis.

Tissues were homogenized at 4°C in 20 mM Tris (pH 7.4), 5 mM EDTA (pH 8.0), 10 mM sodium pyrophosphate, 1% Triton X, phosphatase inhibitor (Calbiochem, California, USA) and proteinase inhibitor (Sigma). The homogenates were centrifuged, and the resulting supernatants (20 µg of protein) were fractionated by SDS-PAGE. Immunoblot analysis was then performed with specific antibodies indicated in Table 2. Immune complexes were visualized with horseradish peroxidase–conjugated secondary antibodies (Santa Cruz Biotechnology, California, USA) and enhanced chemiluminescence reagents (GE Healthcare, Tokyo, Japan). Protein bands were quantified using Image J software (National Institutes of Health, <http://rsbweb.nih.gov/ij>).

Measurement of acetylated PGC-1 α

The red portion of gastrocnemius muscle was homogenized at 4°C in lysis buffer containing 50 mM Tris (pH 7.4), 1 mM EDTA, 150mM potassium chloride, 1% NP40, 5 mM nicotinamide, 1mM sodium butyrate phosphatase inhibitor (Calbiochem) and proteinase inhibitor (Sigma). The muscle lysate (2 mg of protein) was subjected to pre-cleaning with 40 µl of protein G-conjugated sepharose beads (GE Healthcare, Tokyo, Japan), and immunoprecipitated with 4 µg of PGC-1 (H300) antibody (Santa Cruz Biotechnology) and protein A-conjugated sepharose beads (GE Healthcare). The

resulting immunoprecipitate was boiled with 50 μ l of sample buffer containing 125mM Tris-HCl(pH 6.8), 20% Glycerol, 4% SDS, 0.02% Bromophenol Blue and 20% 2-mercaptoethanol and subjected to Western blot analysis with antibody for acetylated-lysine (Cell Signaling Technology, Denvers, MA) or total PGC-1 α (H300).

RNA extraction and quantitative real-time PCR

Total RNA was isolated from tissues with the use of Isogen (Nippon Gene, Wako, Japan), and portions of the RNA (400 ng) were subjected to reverse transcription with an oligo(dT) primer (Sigma) and avian myeloblastosis virus reverse transcriptase (Takara, Shiga, Japan). For quantitative real-time PCR, cDNA was quantified using SYBR Green PCR Master Mix with an ABI 7500 real-time PCR system (Applied Biosystems, Tokyo, Japan) as described previously (22). Data were normalized by the corresponding abundance of acidic ribosomal protein for skeletal muscle and 36B4 for adipose tissue sample. The sequences of the primers are shown in Table 3.

Measurement of plasma metabolites and hormones

Plasma concentrations of glucose, free fatty acids, triglyceride, ketone bodies, insulin, glucagon, corticosterone, IL-6 and irisin in blood samples were measured by kits listed in Table 1.

Chronic infusion of leptin and neutral antibody for IL-6

Recombinant murine leptin (0.5 mg/ml) (PeproTech Inc., Rocky Hill, NJ) or neutral antibody for IL-6 (1 mg/ml) (R&D Systems, Inc., Minneapolis, MN) (31) was delivered subcutaneously with osmotic minipump (Alzet, model 2002, Muromachi Kikai Co., Ltd., Tokyo, Japan) at a rate of 0.5 μ l/hr for 14 days. Osmotic minipump was implanted subcutaneously under ketamine (100 mg/kg of body mass) and xylazine (10 mg/kg) anesthesia. The control group received phosphate-buffered saline delivered with the same type of pump. STZ (200 mg/kg) or vehicle was then injected i.p. twice on the 2nd and 4th day after implantation of osmotic minipump. Body weight and plasma concentrations of glucose and insulin were monitored daily. Two weeks after the implantation of minipump, mice were decapitated, and blood and tissue samples were collected.

Statistical analysis

Data are presented as means \pm standard error of the mean (SEM). Statistical comparisons among multiple groups were performed by analysis of variance (ANOVA) followed by Tukey's HSD post hoc test. Statistical analysis between 2 groups was performed by Student's t test. A *P* value of <0.05 was considered statistically significant.

RESULTS

STZ-induced IDDM activates AMPK in skeletal muscle.

I first examined whether AMPK in skeletal muscle is activated in mice by STZ-induced IDDM. STZ-treated WT mice increased Thr172 phosphorylation of AMPK in soleus muscle (red type of skeletal muscle) and extensor digitorum longus (EDL) (mixed type of skeletal muscle) (Fig. 1A). Ser79 phosphorylation of ACC, which is phosphorylated by AMPK, also increased in soleus muscle in STZ-treated WT mice (Fig 1B). Preferential expression of the mutated $\alpha 1$ catalytic subunit increased the protein abundance of $\alpha 1$ AMPK in hindlimb muscles including soleus, red and white portions of gastrocnemius, and EDL in DN-AMPK mice, but not other tissues such as heart muscle, inguinal (Ing) and epididymal (Epi) WAT, interscapular brown adipose tissue (BAT), pancreas, spleen or the brain (Fig. 1B and C). In contrast, as reported previously (29), the abundance of $\alpha 2$ catalytic subunit of AMPK decreased in those skeletal muscles, probably due to the reason that single subunits of AMPK not consisted of heterotrimer are degraded (29). In parallel to the AMPK activation, Ser79 phosphorylation of ACC did not increase in soleus muscle in STZ-treated DN-AMPK mice (Fig. 1B).

STZ treatment decreased plasma concentration of insulin (Fig. 2A) and Ser473 phosphorylation of AKT in soleus muscle (Fig. 2B) in both STZ-treated WT and DN-AMPK mice. However, the plasma glucose concentration was significantly lower in STZ-treated DN-AMPK

mice than that in STZ-treated WT mice (Fig. 2C). Thus, preferential inhibition of AMPK activity in skeletal muscle improved hyperglycemia, although plasma insulin level remains low and its signaling in skeletal muscle was inhibited.

Preferential expression of DN-AMPK in skeletal muscle improves body weight loss, hyperphagia, decreased survival rate, and tissue weight loss in STZ-induced IDDM.

WT mice decreased body weight by STZ treatment (Fig. 3A). However, it significantly improved in STZ-treated DN-AMPK mice. STZ-induced hyperphagia was also suppressed in STZ-treated DN-AMPK mice (Fig. 3B). Furthermore, all STZ-treated DN-AMPK mice survived at 2 weeks after the 1st injection of STZ, while only 35.7% of STZ-treated WT mice did (Fig. 3C).

STZ-treated DN-AMPK mice also significantly recovered tissue weight of soleus and gastrocnemius muscle, compared with those in STZ-treated WT mice (Fig. 3D). Moreover, decreased tissue weight of epididymal (Epi) and inguinal (Ing) WAT as well as interscapular BAT by STZ treatment significantly recovered in STZ-treated DN-AMPK mice (Fig. 3E). These data suggest that inhibition of AMPK activation in skeletal muscle improved STZ-induced atrophy of skeletal muscle and adipose tissue, and body weight loss, increasing survival rate.

Preferential expression of DN-AMPK in skeletal muscle improves systemic glucose and lipid metabolism.

At two weeks after 2nd injection of STZ, STZ-treated WT mice increased plasma concentration of free fatty acids, triglyceride and ketone bodies, and STZ-treated DN-AMPK mice completely returned to the control levels (Fig. 4A). Plasma concentration of norepinephrine, epinephrine and corticosterone increased in STZ-treated WT mice but not STZ-treated DN-AMPK mice (Fig. 4B). In contrast, the concentration of plasma glucagon remained high in STZ-treated DN-AMPK mice, similar to that in STZ-treated WT mice (Fig. 4B). Thus, partial improvement of plasma glucose level in STZ-treated DN-AMPK mice is due to hyperglucagonemia in the mice (Fig. 2C).

To further investigate the effect of muscle specific DN-AMPK expression on systemic glucose and lipid metabolism, I performed glucose tolerance test (GTT) and pyruvate tolerance test, and fat (triolein) loading test after four hours fasting. STZ-treated WT mice largely increased plasma glucose concentration in response to GTT (Fig. 5A). However, STZ-treated DN-AMPK mice significantly improved the plasma glucose level (Fig. 5A). Increase in plasma free fatty acids and triglyceride levels in response to triolein ingestion, also improved in STZ-treated DN-AMPK mice (Fig. 5C). During the experiments, plasma insulin concentration was low in STZ-treated DN-AMPK mice, similar to that in STZ-treated WT mice (Fig. 5B and D). Furthermore, pyruvate tolerance test,

which is associated with gluconeogenic activity in the liver, revealed that increased plasma glucose level in response to pyruvate injection, significantly improved in STZ-treated DN-AMPK mice (Fig. 5E). mRNA abundance of phosphoenolpyruvate carboxylase (PEPCK) decreased in the liver in STZ-treated DN-AMPK mice (Fig. 5F). These data suggest that the inhibition of AMPK activity in skeletal muscle improved systemic glucose and lipid metabolism even though plasma insulin level remains low.

Preferential expression of DN-AMPK in skeletal muscle inhibits activation of AMPK-related signals in skeletal muscle in response to STZ-induced IDDM.

Fig. 1B revealed that IDDM stimulates ACC phosphorylation in skeletal muscle in parallel to the AMPK activation. I further examined other downstream signals related to AMPK in soleus muscle. STZ-treated WT mice increased mRNA abundance of NAMPT and SIRT1 in soleus muscle, but those changes were reversed in STZ-treated DN-AMPK mice (Fig. 6A). Furthermore, abundance of the acetylated PGC-1 α in red portion of gastrocnemius muscle decreased in STZ-treated WT but not STZ-treated DN-AMPK mice (Fig. 6B).

Autophagy plays an important role in adaptive response of skeletal muscle in energy crisis such as long-term starvation (32-34). AMPK regulates autophagy via direct phosphorylation

(Ser555) of ULK1 and then increase in the protein abundance of LC3-II (17-19). STZ-treated WT mice increased the phosphorylation of ULK1 and protein abundance of LC3-II in soleus muscle, but those changes were reversed in STZ-treated DN-AMPK mice (Fig. 6C and D).

AMPK has been shown to inhibit protein synthesis by increasing phosphorylation (Ser1387) of TSC2 (Tuberous sclerosis complex) and decreasing mTOR signal (15, 16). STZ-treated WT mice increased the phosphorylation of TSC2 (Ser1387), and it decreased that of S6K (Thr389) in soleus muscle. Those were returned to the control levels in STZ-treated DN-AMPK mice (Fig. 6E and F).

Preferential expression of DN-AMPK in skeletal muscle reverses AMPK activation and altered gene expressions in WAT in STZ-induced IDDM

To explore the mechanism for atrophy of WAT in IDDM mice, I examined AMPK activation and gene expressions in WAT in STZ-treated WT and DN-AMPK mice. Similar to that in skeletal muscle, AMPK was activated in Ing WAT in STZ-treated WT mice, and the activation was blunted in STZ-treated DN-AMPK mice (Fig. 7A). AMPK has been shown to inhibit lipogenesis and its related gene expression in adipocytes (35). mRNA abundance of fatty acid synthase (FAS) and lipoprotein lipase (LPL) was decreased in inguinal (Ing) WAT in IDDM WT mice, but those

expressions were significantly recovered in STZ-treated DN-AMPK mice (Fig. 7B). Moreover, unexpectedly, I found that STZ-treated WT mice increased gene expression of UCP1 and Cidea (cell-death-inducing DFF45-like effector A) in Ing WAT, and those expressions were suppressed in STZ-treated DN-AMPK (Fig. 7B). These results suggest that atrophy of WAT is induced by suppression of lipogenesis and probably enhanced by increased expressions of thermogenic protein UCP1 in WAT.

STZ-induced IDDM increases expression of myokines in skeletal muscle in AMPK-dependent manner

To explore the mechanism by which suppression of AMPK activation in skeletal muscle improved “lipoatrophy” in STZ-induced IDDM, I examined the expression of myokines that affect adipocyte metabolism. Recent study revealed that a novel myokine, irisin, is produced from FNDC5 (fibronectin type III domain containing 5) in skeletal muscle in PGC-1 α -dependent manner (27), and induces UCP1 and related gene expressions in subcutaneous WAT. Consistent with PGC-1 α activation in skeletal muscle, STZ-treated WT mice increased abundance of FNDC5 protein in soleus muscle (Fig. 8A) and concentration in plasma irisin (Fig. 8B). Those were completely reversed to the control levels in STZ-treated DN-AMPK mice.

IL-6 is another myokine released from skeletal muscle, and stimulates lipolysis in WAT (25, 26). IL-6 has been reported to activate AMPK (26). STZ-treated WT mice increased abundance of IL-6 protein in soleus muscle (Fig. 8C) and concentration in plasma IL-6 (Fig. 8D), but those were decreased in STZ-treated DN-AMPK mice. I examined plasma concentration of IL-15, which has been reported to be released from skeletal muscle (36). However, IL-15 did not increase in plasma in STZ-treated WT mice (data not shown).

Plasma concentrations of leptin and adiponectin in STZ-treated WT and DN-AMPK mice

Leptin is secreted from adipocytes and its secretion is closely associated with amount of WAT. Leptin has been shown to stimulate glucose utilization in skeletal muscle via sympathetic nerve and β -adrenergic receptor in the tissue (20-22). Furthermore, chronic leptin treatment improves metabolic changes in IDDM including STZ-induced diabetes through the central nervous system (23, 24, 37, 38). Another adipocyte hormone adiponectin also stimulates glucose and lipid utilization in skeletal muscle and suppresses glucose production in the liver (39). I found that concentration of plasma leptin was decreased in STZ-treated WT mice and it was significantly recovered in STZ-treated DN-AMPK mice (Fig. 9A). Plasma concentration of high molecular weight of adiponectin did not alter in STZ-treated WT mice (Fig. 9B), but it increased in STZ-treated DN-AMPK mice

(Fig. 9B).

Chronic infusion of leptin or neutral antibody for IL-6 improves metabolic abnormalities in STZ-induced IDDM

To explore the role of leptin and IL-6 in metabolic changes in STZ-induced IDDM, I infused leptin or neutral antibody for IL-6 into STZ-induced IDDM C57Bl/6J mice for 2 weeks, using osmotic minipump. Infusion of leptin decreased plasma concentration of glucose to the control level without STZ treatment (Fig. 10A). Infusion of IL-6 antibody also decreased the plasma concentration of glucose (Fig. 10A). Furthermore, concentration of plasma free fatty acids returned to the control level by infusion of leptin and IL-6 antibody (Fig. 10A).

Infusion of leptin increased the concentration of plasma leptin to approximate 30 ng/ml on 3rd day after the implantation of minipump (data not shown) and kept the concentration upto the end of experiment (2 weeks) (Fig. 10B). Consistent with the increased amount of adipose tissues, infusion of IL-6 antibody significantly increased plasma leptin concentration compared with that of STZ treatment alone (STZ + vehicle: 0.12 ± 0.01 ng/ml; STZ + IL-6 antibody: 4.18 ± 0.57 ng/ml) (Fig. 10B). Concentrations of plasma IL-6 and irisin were decreased by infusion of IL-6 antibody and leptin (Fig. 10B). In contrast, concentrations of plasma insulin were low after infusion of IL-6

antibody and leptin, similar to that after STZ treatment alone (Fig. 10B).

I next examined tissue amount of skeletal muscle, WAT and BAT after infusion of leptin, or antibody for IL-6 in STZ-induced IDDM. All of the infusions increased the amount of soleus, EDL and gastrocnemius muscle (Fig. 10C). Furthermore, infusion of antibody for IL-6 increased the amount of Epi and Ing WAT and BAT (Fig. 10C). Infusion of leptin also recovered the amount of those adipose tissues slightly (Fig. 10C). The smaller increase in adipose tissue amount by leptin infusion than that of infusion of IL-6 antibody may be due to the catabolic effect of leptin on lipid metabolism in adipose tissue (Fig. 10C). Together, these results suggest that STZ-induced IDDM activates AMPK in skeletal muscle and induces muscle atrophy, thereby increasing IL-6 and irisin production (Fig. 11). Increase in plasma level of IL-6 stimulates catabolic process in adipose tissue, then decreasing leptin production. Irisin may also induce UCP1 expression and decrease amount of WAT. Decreased concentration of plasma leptin impairs glucose and lipid metabolism in skeletal muscle, and induces a vicious cycle in organ networks.

DISCUSSION

The present data revealed that AMPK in skeletal muscle plays an important role in metabolic changes in STZ-induced IDDM. I found that inhibition of AMPK activation in skeletal muscle improved glucose and lipid metabolism in STZ-induced IDDM. Glucose tolerance, fat loading and pyruvate tolerance tests revealed the improvement of whole body metabolism in IDDM, although plasma insulin level remains low. Furthermore, inhibition of AMPK activation in skeletal muscle significantly prevented atrophy of muscle and adipose tissue, and increased survival rate. I found that IL-6 and adipocyte hormone leptin were possibly mediators involved in the metabolic changes in STZ-induced IDDM. Thus, the present data suggest that metabolic abnormalities in STZ-induced IDDM are caused by a vicious cycle in organ networks including muscle and adipose tissue.

Leptin is an adipocyte-derived hormone that plays an important role in glucose metabolism in peripheral tissues including skeletal muscle and BAT, as well as energy metabolism in mammals (20-22). Treatment with leptin ameliorates diabetes in both lipodystrophic mice and humans (40, 41) as well as type I (23, 24) and obesity-unrelated type II diabetes in rodents (42). In the present study, I found that suppression of AMPK activity in skeletal muscle increases plasma leptin level. Furthermore, leptin infusion improved metabolic abnormalities and atrophy of muscle and adipose tissues. IL-6 antibody infusion also improved those metabolic changes in STZ-induced IDDM, increasing plasma leptin level. Thus, the results suggest that low plasma leptin level in IDDM

associated with “lipoatrophy” caused the metabolic abnormalities in STZ-induced IDDM. Recovery of tissue amount of skeletal muscles and BAT by leptin plays a role in the improvement of glucose and lipid metabolism in STZ-induced IDDM, because BAT as well as skeletal muscle is an important organ for glucose metabolism in rodents. BAT has been shown to secrete FGF21 (fibroblast growth factor 21) that regulates whole body glucose homeostasis (43). Recent studies demonstrate that leptin stimulates glucose uptake and fatty acid oxidation in skeletal muscle through the hypothalamus and sympathetic nervous system (20-22, 44). The increase in glucose uptake and fatty acid oxidation by leptin appears to be mediated by distinct intracellular signals in muscle; glucose uptake of muscle in response to leptin is mediated by β -adrenergic receptor (21, 22), while fatty acid oxidation is mediated by α -adrenergic receptor and activation of muscle AMPK (44). Activation of AMPK thus mediates leptin-induced fatty acid oxidation but not glucose uptake in skeletal muscle. Because impairment of glucose utilization inhibits oxidation of acetyl-CoA in TCA cycle, decrease of plasma level of leptin as well as insulin may impair both glucose and lipid metabolism in skeletal muscle in STZ-induced IDDM even though AMPK is activated in the tissue. Instead, activation of AMPK probably causes severe catabolic process in skeletal muscle by inhibiting protein synthesis and activating autophagy. In the present study, I used a single dose of leptin that increased plasma leptin concentration approximately 3-folds. In future study, I need to examine whether physiological

concentration of leptin recovers those metabolic abnormalities in STZ-induced IDDM. Adiponectin has also been reported to stimulate glucose and lipid metabolism in skeletal muscle and inhibits glucose production in the liver (39). The present data revealed that plasma adiponectin level increased in STZ-treated DN-AMPK mice, while it did not change in STZ-treated WT mice. The increased level of plasma adiponectin may improve glucose and lipid metabolism in the mice, while the mechanism by which plasma concentration of high molecular weight adiponectin increased in STZ-treated DN-AMPK mice. Thus, the present results suggest that inhibition of AMPK activation in skeletal muscle bunts a vicious cycle in IDDM through correcting organ networks for metabolic regulation.

IL-6 is a myokine that is released from skeletal muscle and stimulates lipolysis in adipose tissue (26). I found that STZ-induced IDDM increased IL-6 production in skeletal muscle and its plasma concentration, and these are completely reversed by suppression of AMPK activation in skeletal muscle. Infusion of IL-6 antibody improved hyperglycemia, plasma level of free fatty acids and atrophy of adipose tissues and skeletal muscle. A preliminary result of Dr. Sato in Division of Endocrinology and Metabolism in National Institute for Physiological Sciences, have shown that chronic treatment with IL-6 enhances UCP1 expression by norepinephrine and decreased triglyceride amount in primary culture of white adipocytes isolated from subcutaneous WAT in mice.

In the present study, concentration of plasma norepinephrine and epinephrine increased in STZ-treated WT mice but not in STZ-treated DN-AMPK mice. It is possible that increased concentration of plasma IL-6 as well as norepinephrine and epinephrine enhanced UCP1 gene expression as well as lipolysis in WAT. At present, it remains unknown the mechanisms by which IL-6, norepinephrine, epinephrine, and corticosterone are increased in STZ-induced IDDM.

Irisin is also a novel myokine that is released from skeletal muscle in PGC-1 α -dependent manner and induces UCP1 expression in subcutaneous WAT (25). While physiological relevance of irisin for UCP1 expression and its role in energy homeostasis in WAT are still unknown, the present data suggest that irisin may increase UCP1 expression in WAT and is involved in the decreased amount of WAT in STZ-induced IDDM mice. In support of this, my preliminary results showed that infusion of neutral antibody for irisin improved hyperglycemia and atrophy of skeletal muscle and adipose tissues, similar to those of infusion of IL-6 antibody (data not shown). Furthermore, I have examined the effect of STZ-induced IDDM on those metabolic parameters in UCP1-knockout (KO) mice. The preliminary results revealed that UCP1-KO mice improved the metabolic abnormalities in STZ-induced IDDM, compared with those in WT mice (data not shown). Interestingly, I found that infusion of IL-6 antibody decreased plasma irisin level as well as IL-6 in STZ-induced IDDM. It is speculated that infusion of IL-6 antibody improved metabolic abnormalities in skeletal muscle

via improvement of metabolic changes in adipose tissues. Alternatively, infusion of IL-6 antibody may inhibit IL-6-induced AMPK activation in skeletal muscle and thereby decrease irisin secretion.

Pyruvate tolerance test revealed that inhibition of AMPK activation in skeletal muscle improved gluconeogenesis from pyruvate to glucose in STZ-treated DN-AMPK mice. Increased mRNA abundance of PEPCK in the liver in STZ-induced IDDM significantly decreased in STZ-treated DN-AMPK mice. The improvement of gluconeogenic activity in the liver is probably mediated by the decreased level of plasma norepinephrine, epinephrine and corticosterone. Furthermore, the recovery of plasma leptin level and increased plasma adiponectin level may decrease glucose production in the liver. Infusion of leptin has been reported to decrease mRNA abundance of PEPCK in the liver in IDDM mice (24). Partial recovery on GTT and pyruvate tolerance test in STZ-treated DN-AMPK mice may be due to the increased level of plasma glucagon. Infusion of pharmacological dose of leptin has been shown to reduce plasma glucagon level and improve hyperglycemia completely (24). Further investigation is necessary to explore the effects of several dose of leptin on plasma level of glucagon as well as glucose.

Collectively, I found that inhibition of AMPK activation in skeletal muscle improves metabolic abnormalities in STZ-induced IDDM. Furthermore, infusion of neutral antibody for IL-6 as well as leptin improved the metabolic abnormalities. These results suggest that the metabolic

changes in IDDM are caused by a vicious cycle of organ networks in IDDM, rather than insulin deficiency itself. Insulin treatment has been assumed to be only a therapy to prevent hyperglycemia during feeding. However, the present results of GTT, fat loading and pyruvate tolerance tests showed that inhibition of AMPK activation in skeletal muscle prevented the increase in plasma lipids as well as glucose in STZ-induced IDDM. Therefore, the suppression of AMPK activity and IL-6 signals, as well as leptin infusion therapy, probably reduces the dose of insulin required for IDDM therapy. The present study provides a novel insight for important role of organ networks in metabolic regulation in IDDM.

ACKNOWLEDGMENTS

I would like to express my sincere appreciation to Drs. Yasuhiko Minokoshi, Shiki Okamoto, Chitoku Toda for their generous supports and valuable guidance trough this study. I would also like to thank Kumiko Saito and Kei Nagatani for helpful assistance and Dr. Sato for providing useful preliminary results. I wish to thank all the member of Division of Endocrinology and Metabolism for their supports, and inspiring discussion.

REFERENCES

1. Daneman D. (2006) Type 1 diabetes. *Lancet* 367:847–858.
2. Cryer PE. (2004) Diverse causes of hypoglycemia-associated autonomic failure in diabetes. *N Engl J Med.* 350:2272–2279.
3. Maahs DM, Rewers M. (2006) Mortality and renal disease in type 1 diabetes mellitus—Progress made, more to be done. *J Clin Endocrinol Metab.* 91:3757–3759.
4. Steffes MW, Sibley S, Jackson M, Thomas W. (2003) Beta-cell function and the development of diabetes-related complications in the diabetes control and complications trial. *Diabetes Care.* 26:832–836.
5. Bluestone JA, Herold K, Eisenbarth G. (2010) Genetics, pathogenesis and clinical interventions in type 1 diabetes. *Nature.* 464:1293–1300.
6. Liu HY, Cao SY, Hong T, Han J, Liu Z, Cao W. (2009) Insulin is a stronger inducer of insulin resistance than hyperglycemia in mice with type 1 diabetes mellitus (T1DM). *J Biol Chem.* 284:27090–27100.
7. Larsen J, Brekke M, Sandvik L, Arnesen H, Hanssen KF, Dahl-Jorgensen K. (2002) Silent coronary atheromatosis in type 1 diabetic patients and its relation to long-term glycemic control. *Diabetes.* 51:2637–2641.
8. Orchard TJ, Olson JC, Erbey JR, Williams K, Forrest KY, Smithline Kinder L, Ellis D, Becker DJ. (2003) Insulin resistance-related factors, but not glycemia, predict coronary artery disease in type 1 diabetes: 10-year follow-up data from the Pittsburgh Epidemiology of Diabetes Complications Study. *Diabetes Care.* 26:1374–1379.
9. Hardie DG, Ross FA, Hawley SA. (2012) AMPK: a nutrient and energy sensor that maintains energy homeostasis. *Nat Rev Mol Cell Biol.* 13:251-262.
10. Xiao B, Sanders MJ, Underwood E, Heath R, Mayer FV, Carmena D, Jing C, Walker PA, Eccleston JF, Haire LF, Saiu P, Howell SA, Aasland R, Martin SR, Carling D, Gamblin SJ. (2011) Structure of mammalian AMPK and its regulation by ADP. *Nature.* 472:230-233.
11. Merrill GF, Kurth EJ, Hardie DG, Winder WW. (1997) AICAR decreases malonyl-CoA and increases fatty acid oxidation in skeletal muscle of the rat. *Am. J. Physiol. Endocrine. Metab.* 273:E1107–E1112.
12. Fulco M, Cen Y, Zhao P, Hoffman EP, McBurney MW, Sauve AA, Sartorelli V. (2008) Glucose restriction inhibits skeletal myoblast differentiation by activating SIRT1 through AMPK-mediated regulation of Nampt. *Dev Cell.* 14:661-673.

13. Cantó C, Gerhart-Hines Z, Feige JN, Lagouge M, Noriega L, Milne JC, Elliott PJ, Puigserver P, Auwerx J. (2009) AMPK regulates energy expenditure by modulating NAD⁺ metabolism and SIRT1 activity. *Nature*. 458:1056-1060.
14. Cantó C, Jiang LQ, Deshmukh AS, Matakı C, Coste A, Lagouge M, Zierath JR, Auwerx J. (2010) Interdependence of AMPK and SIRT1 for metabolic adaptation to fasting and exercise in skeletal muscle. *Cell Metab*. 11:213-219.
15. Inoki K, Zhu T, Guan KL. (2003) TSC2 mediates cellular energy response to control cell growth and survival. *Cell*. 115:577-590.
16. Gwinn DM, Shackelford DB, Egan DF, Mihaylova MM, Mery A, Vasquez DS, Turk BE, Shaw RJ. (2008) AMPK phosphorylation of raptor mediates a metabolic checkpoint. *Mol Cell*. 30:214-226.
17. Egan DF, Shackelford DB, Mihaylova MM, Gelino S, Kohnz RA, Mair W, Vasquez DS, Joshi A, Gwinn DM, Taylor R, Asara JM, Fitzpatrick J, Dillin A, Viollet B, Kundu M, Hansen M, Shaw RJ. (2011) Phosphorylation of ULK1 (hATG1) by AMP-activated protein kinase connects energy sensing to mitophagy. *Science*. 331:456-461.
18. Kim J, Kundu M, Viollet B, Guan KL. (2011) AMPK and mTOR regulate autophagy through direct phosphorylation of Ulk1. *Nat Cell Biol*. 13:132-141.
19. Sanchez AM, Csibi A, Raibon A, Cornille K, Gay S, Bernardi H, Candau R. (2012) AMPK promotes skeletal muscle autophagy through activation of forkhead FoxO3a and interaction with Ulk1. *J Cell Biochem*. 113:695-710.
20. Minokoshi Y, Haque MS, Shimazu T. (1999) Microinjection of leptin into the ventromedial hypothalamus increases glucose uptake in peripheral tissues in rats. *Diabetes*. 48:287-291.
21. Haque MS, Minokoshi Y, Hamai M, Iwai M, Horiuchi M, Shimazu T. (1999) Role of the sympathetic nervous system and insulin in enhancing glucose uptake in peripheral tissues after intrahypothalamic injection of leptin in rats. *Diabetes*. 48:1706-1712.
22. Toda C, Shiuchi T, Lee S, Yamato-Esaki M, Fujino Y, Suzuki A, Okamoto S, Minokoshi Y. (2009) Distinct effects of leptin and a melanocortin receptor agonist injected into medial hypothalamic nuclei on glucose uptake in peripheral tissues. *Diabetes*. 58:2757-2765.
23. Denroche HC, Levi J, Wideman RD, Sequeira RM, Huynh FK, Covey SD, Kieffer TJ. (2011) Leptin therapy reverses hyperglycemia in mice with streptozotocin-induced diabetes, independent of hepatic leptin signaling. *Diabetes*. 60:1414-1423.
24. Wang MY, Chen L, Clark GO, Lee Y, Stevens RD, Ilkayeva OR, Wenner BR, Bain JR, Charron MJ, Newgard CB, Unger RH. (2010) Leptin therapy in insulin-deficient type I diabetes. *Proc Natl Acad Sci U S A*. 107:4813-4819.

25. Pedersen BK, Febbraio MA. (2008) Muscle as an endocrine organ: focus on muscle-derived interleukin-6. *Physiol Rev.* 88:1379–1406.
26. Wan Z, Ritchie I, Beaudoin MS, Castellani L, Chan CB, Wright DC. (2012) IL-6 Indirectly Modulates the Induction of Glyceroneogenic Enzymes in Adipose Tissue during Exercise. *PLoS One.* 7:e41719
27. Boström P, Wu J, Jedrychowski MP, Korde A, Ye L, Lo JC, Rasbach KA, Boström EA, Choi JH, Long JZ, Kajimura S, Zingaretti MC, Vind BF, Tu H, Cinti S, Højlund K, Gygi SP, Spiegelman BM. (2012) A PGC1- α -dependent myokine that drives brown-fat-like development of white fat and thermogenesis. *Nature.* 481:463-468.
28. Wu J, Boström P, Sparks LM, Ye L, Choi JH, Giang AH, Khandekar M, Virtanen KA, Nuutila P, Schaart G, Huang K, Tu H, van Marken Lichtenbelt WD, Hoeks J, Enerbäck S, Schrauwen P, Spiegelman BM. (2012) Beige adipocytes are a distinct type of thermogenic fat cell in mouse and human. *Cell.* 150:366-376.
29. Miura S, Kai Y, Kamei Y, Bruce CR, Kubota N, Febbraio MA, Kadowaki T, Ezaki O. (2009) Alpha2-AMPK activity is not essential for an increase in fatty acid oxidation during low-intensity exercise. *Am J Physiol Endocrinol Metab.* 296, E47–E55.
30. Kotani K, Peroni OD, Minokoshi Y, Boss O, Kahn BB. (2004) GLUT4 glucose transporter deficiency increases hepatic lipid production and peripheral lipid utilization. *J Clin Invest.* 114:1666-1675.
31. Inoue H, Ogawa W, Asakawa A, Okamoto Y, Nishizawa A, Matsumoto M, Teshigawara K, Matsuki Y, Watanabe E, Hiramatsu R, Notohara K, Katayose K, Okamura H, Kahn CR, Noda T, Takeda K, Akira S, Inui A, Kasuga M. (2006) Role of hepatic STAT3 in brain-insulin action on hepatic glucose production. *Cell Metab.* 3:267-275.
32. Komatsu M, Waguri S, Ueno T, Iwata J, Murata S, Tanida I, Ezaki J, Mizushima N, Ohsumi Y, Uchiyama Y, Kominami E, Tanaka K, Chiba T. (2005) Impairment of starvation-induced and constitutive autophagy in Atg7-deficient mice. *J Cell Biol.* 169: 425–434.
33. Mammucari C, Milan G, Romanello V, Masiero E, Rudolf R, Del Piccolo P, Burden SJ, Di Lisi R, Sandri C, Zhao J, Goldberg AL, Schiaffino S, Sandri M. (2007) FoxO3 controls autophagy in skeletal muscle in vivo. *Cell Metab.* 6:458-471.
34. Lokireddy S, Wijesoma IW, Teng S, Bonala S, Gluckman PD, McFarlane C, Sharma M, Kambadur R. (2012) The ubiquitin ligase Mul1 induces mitophagy in skeletal muscle in response to muscle-wasting stimuli. *Cell Metab.* 16:613-624.

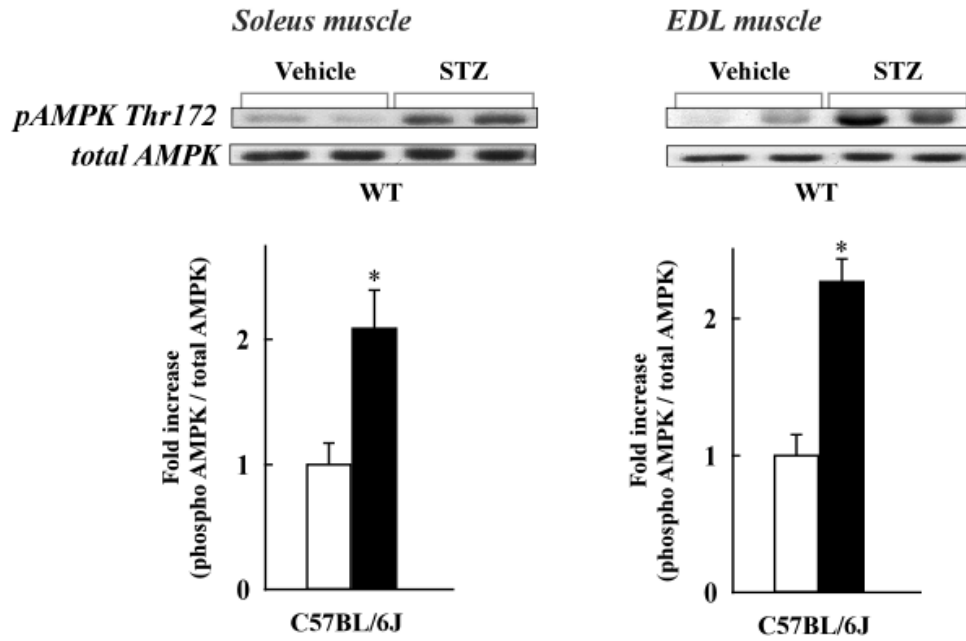
35. Sullivan JE, Brocklehurst KJ, Marley AE, Carey F, Carling D, Beri RK. (1994) Inhibition of lipolysis and lipogenesis in isolated rat adipocytes with AICAR: a cell-permeable activator of AMP-activated protein kinase. *FEBS Lett.* 353:33–36
36. Quinn LS. (2008) Interleukin-15: a muscle-derived cytokine regulating fat-to-lean body composition. *J Anim Sci.* 86:E75-83
37. Yu X, Park BH, Wang MY, Wang ZV, Unger RH. (2008) Making insulin-deficient type 1 diabetic rodents thrive without insulin. *Proc Natl Acad Sci U S A.* 105:14070-14075.
38. Fujikawa T, Chuang JC, Sakata I, Ramadori G, Coppari R. (2010) Leptin therapy improves insulin-deficient type 1 diabetes by CNS-dependent mechanisms in mice. *Proc Natl Acad Sci U S A.* 107:17391-17396.
39. Yamauchi T, Nio Y, Maki T, Kobayashi M, Takazawa T, Iwabu M, Okada-Iwabu M, Kawamoto S, Kubota N, Kubota T, Ito Y, Kamon J, Tsuchida A, Kumagai K, Kozono H, Hada Y, Ogata H, Tokuyama K, Tsunoda M, Ide T, Murakami K, Awazawa M, Takamoto I, Froguel P, Hara K, Tobe K, Nagai R, Ueki K, Kadowaki T. (2007) Targeted disruption of AdipoR1 and AdipoR2 causes abrogation of adiponectin binding and metabolic actions. *Nat Med.* 13:332–339
40. Shimomura I, Hammer RE, Ikemoto S, Brown MS, Goldstein JL. (1999) Leptin reverses insulin resistance and diabetes mellitus in mice with congenital lipodystrophy. *Nature.* 401:73–76
41. Oral EA, Simha V, Ruiz E, Andewelt A, Premkumar A, Snell P, Wagner AJ, DePaoli AM, Reitman ML, Taylor SI, Gorden P, Garg A. (2002) Leptin-replacement therapy for lipodystrophy. *N Engl J Med.* 346:570–578
42. Li X, Wu X, Camacho R, Schwartz G, LeRoith D. (2011) Intracerebroventricular leptin infusion improves glucose homeostasis in lean type 2 diabetic MKR mice via hepatic vagal and non-vagal mechanisms. *PLoS ONE.* 6:e17058
43. Stanford KI, Middelbeek RJ, Townsend KL, An D, Nygaard EB, Hitchcox KM, Markan KR, Nakano K, Hirshman MF, Tseng YH, Goodyear LJ. (2013) Brown adipose tissue regulates glucose homeostasis and insulin sensitivity. *J Clin Invest.* 123:215-223.
44. Minokoshi Y, Kim YB, Peroni OD, Fryer LG, Müller C, Carling D, Kahn BB. (2002) Leptin stimulates fatty-acid oxidation by activating AMP-activated protein kinase. *Nature.* 415:339-343.
45. Suzuki A, Okamoto S, Lee S, Saito K, Shiuchi T, Minokoshi Y. (2007) Leptin stimulates fatty acid oxidation and peroxisome proliferator-activated receptor alpha gene expression in mouse

C2C12 myoblasts by changing the subcellular localization of the alpha2 form of AMP-activated protein kinase. *Mol Cell Biol.* 27:4317-4327.

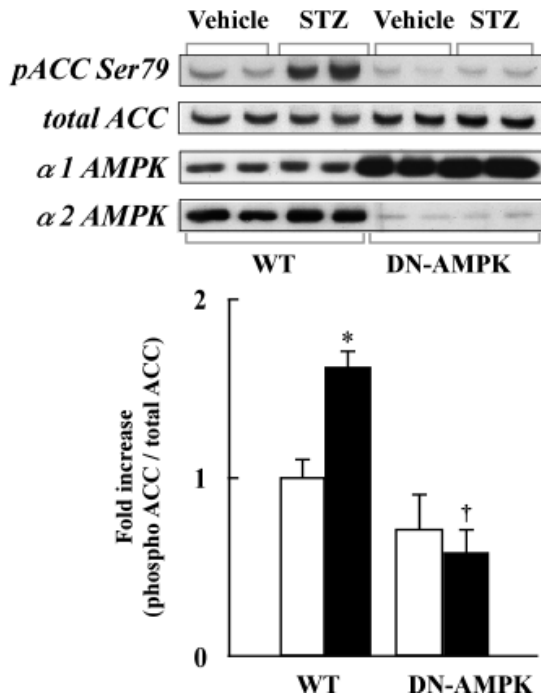
Fig. 1

A

□ Vehicle injection ■ STZ injection



B



C

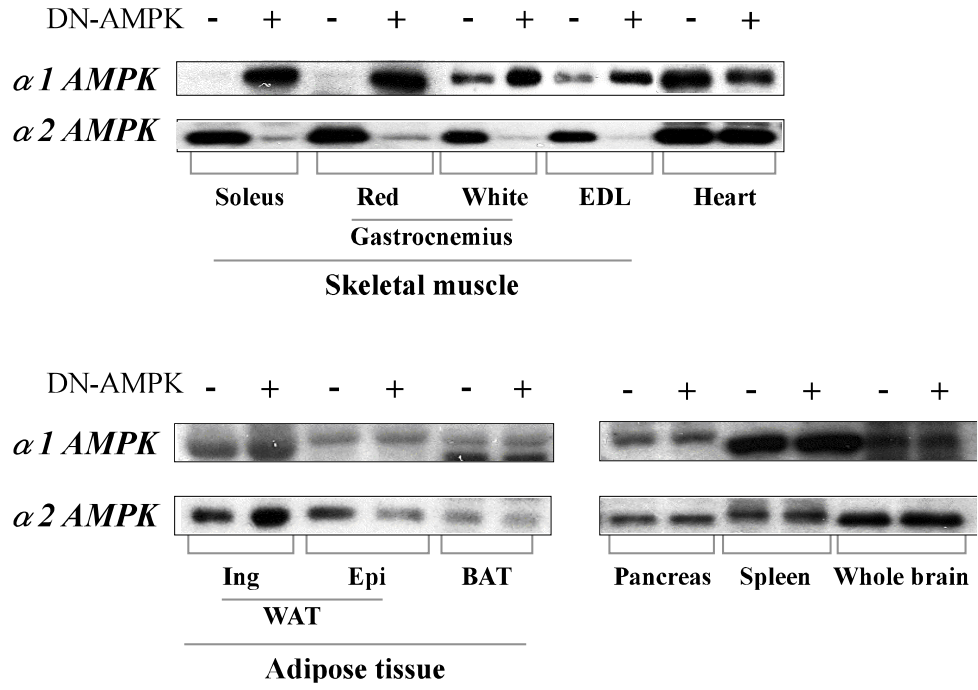


Figure 1. STZ-induced IDDM activates AMPK in skeletal muscle and DN-AMPK mice suppress the activation.

(A) Phosphorylation (Thr172) and total AMPK, and (B) phosphorylation (Ser79) and total ACC, and $\alpha 1$ and $\alpha 2$ AMPK, in soleus muscle in vehicle- and STZ-treated WT mice 2 weeks after 1st injection of STZ. Data of bar graphs were expressed as percentage of total AMPK ($\alpha 1$ plus $\alpha 2$) and ACC, respectively. Representative immunoblots are shown above the quantitative data.

(C) Immunoblots with antibodies for $\alpha 1$ and $\alpha 2$ AMPK in skeletal muscles (soleus, red and white portion of gastrocnemius, and EDL), heart, inguinal (Ing) and epididymal (Epi) WAT, pancreas, spleen and whole brain in WT and DN-AMPK mice.

EDL, extensor digitorum longus. All quantitative data are mean \pm SEM. [n=8-10 for soleus and n=4-5 for EDL in Fig. 1A, n=5-10 for Fig. 1B] Error bar represents the SEM. * $p < 0.05$ versus vehicle-injected mice. † $p < 0.05$ versus STZ-treated WT mice.

Fig. 2

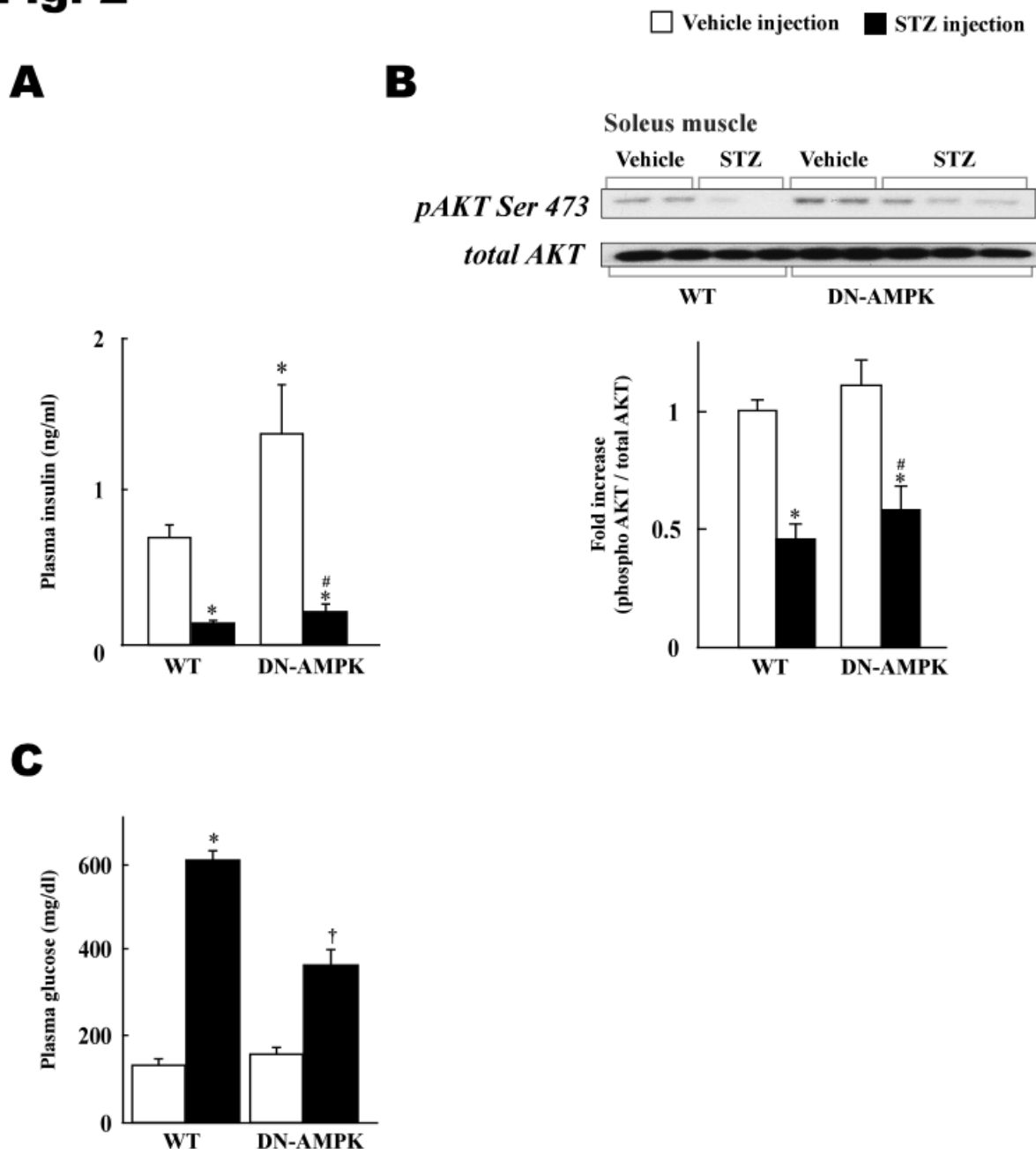


Figure 2. STZ-induced IDDM decreased plasma insulin level, insulin signal in skeletal muscle, and increased plasma glucose level. However, DN-AMPK mice improved the hyperglycemia.

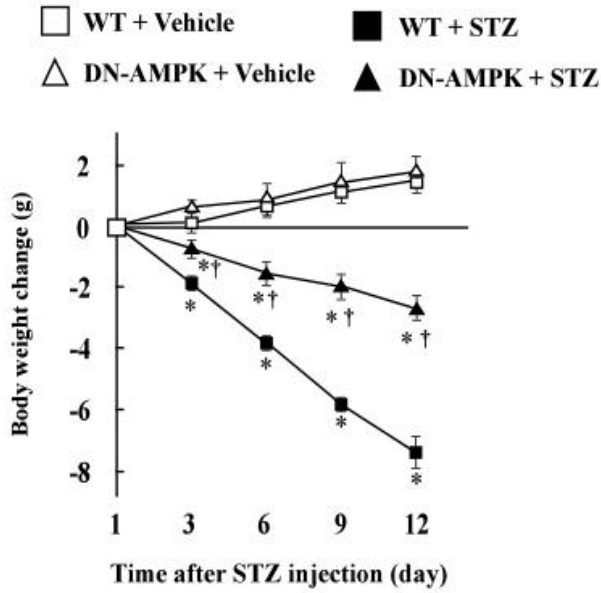
(A) Plasma concentration of insulin, (B) phosphorylation (Tyr473) of AKT, and (C) plasma concentration of glucose, in WT and DN-AMPK mice 2 weeks after 1st injection of STZ or vehicle.

Data of bar graph in (B) were expressed as percentage of total AKT. Representative immunoblots are shown above the quantitative data.

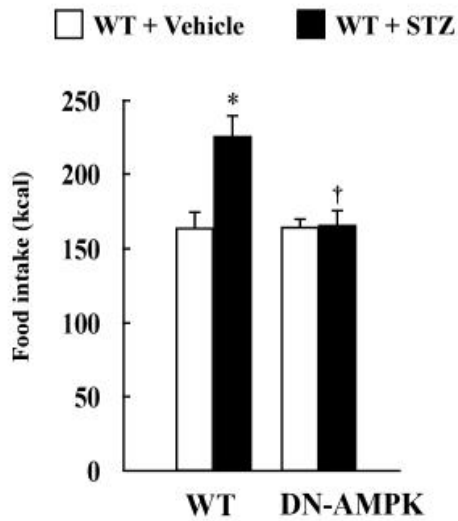
All quantitative data are mean \pm SEM. [n=7-10 in Fig. 2A and 2C, n=5-10 for Fig. 2B] Error bar represents the SEM. * p <0.05 versus vehicle-injected WT mice. # p <0.05 versus vehicle-injected DN-AMPK mice.

Fig. 3

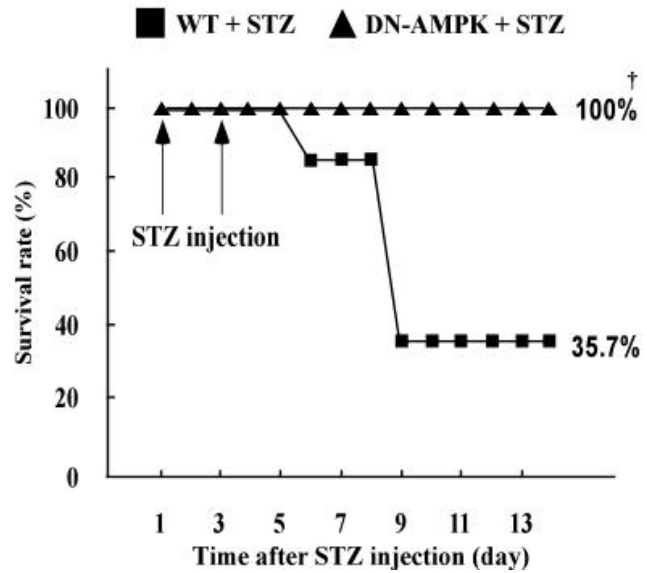
A



B

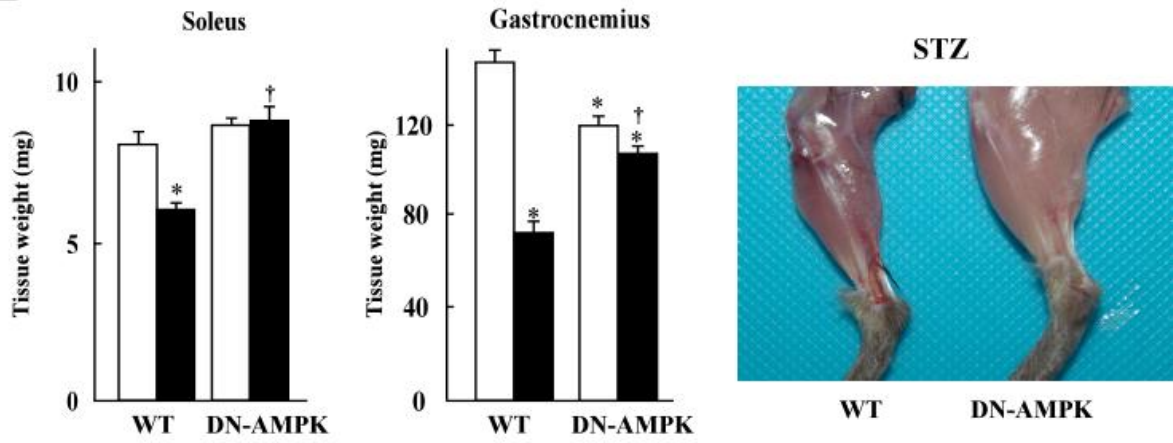


C



□ Vehicle injection ■ STZ injection

D



E

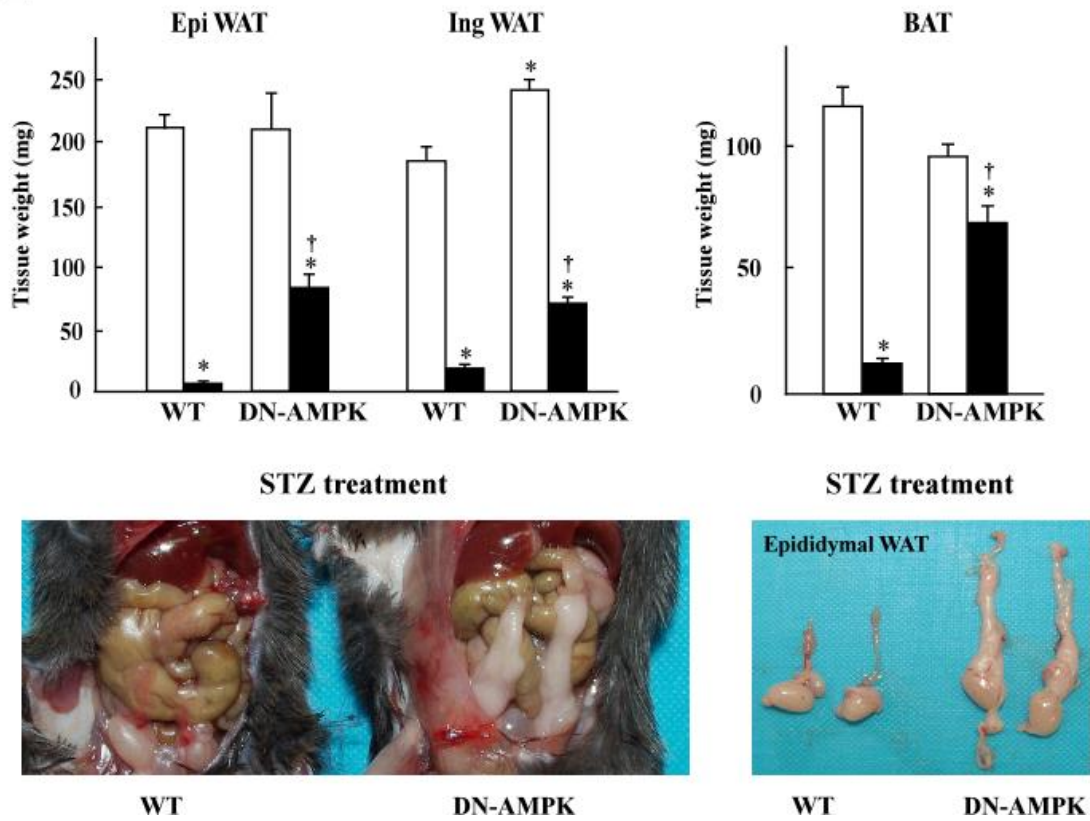


Figure 3. DN-AMPK mice improved body weight loss, hyperphagia, decreased survival rate, and tissue weight loss in STZ-induced IDDM.

(A) Change in body weight. Photograph is WT and DN-AMPK mice at 2 weeks after 1st injection of STZ or vehicle.

(B) Daily food intake 2 weeks after 1st injection of STZ or vehicle.

(C) Survival curve of STZ-treated WT and DN-AMPK mice. Survival rate of STZ-treated WT and DN-AMPK mice at 2 weeks after the 1st injection were significantly different with t-test $^{\dagger}p < 0.05$ versus STZ-injected WT mice.

(D) Tissue weight of skeletal muscles (soleus and gastrocnemius) 2 weeks after 1st injection of STZ or vehicle. Photograph is hindlimbs of STZ-treated WT and DN-AMPK mice.

(E) Tissue weight of adipose tissues [epididymal (Epi) and inguinal (Ing) WAT and BAT], 2 weeks after 1st injection of STZ or vehicle. Photograph is Epi WAT in abdomen (left) and Epi WAT dissected together with testis (right) in STZ-treated WT and DN-AMPK mice.

WT + vehicle: vehicle-treated WT mice; WT + STZ: STZ-treated WT mice; DN-AMPK + vehicle: vehicle-treated DN-AMPK mice; DN-AMPK + STZ: STZ-treated DN-AMPK mice. All quantitative data are mean \pm SEM (n=6-14). Error bar represents the SEM. $*p < 0.05$ versus vehicle-injected WT mice. $^{\dagger}p < 0.05$ versus STZ-injected WT mice.

Fig. 4

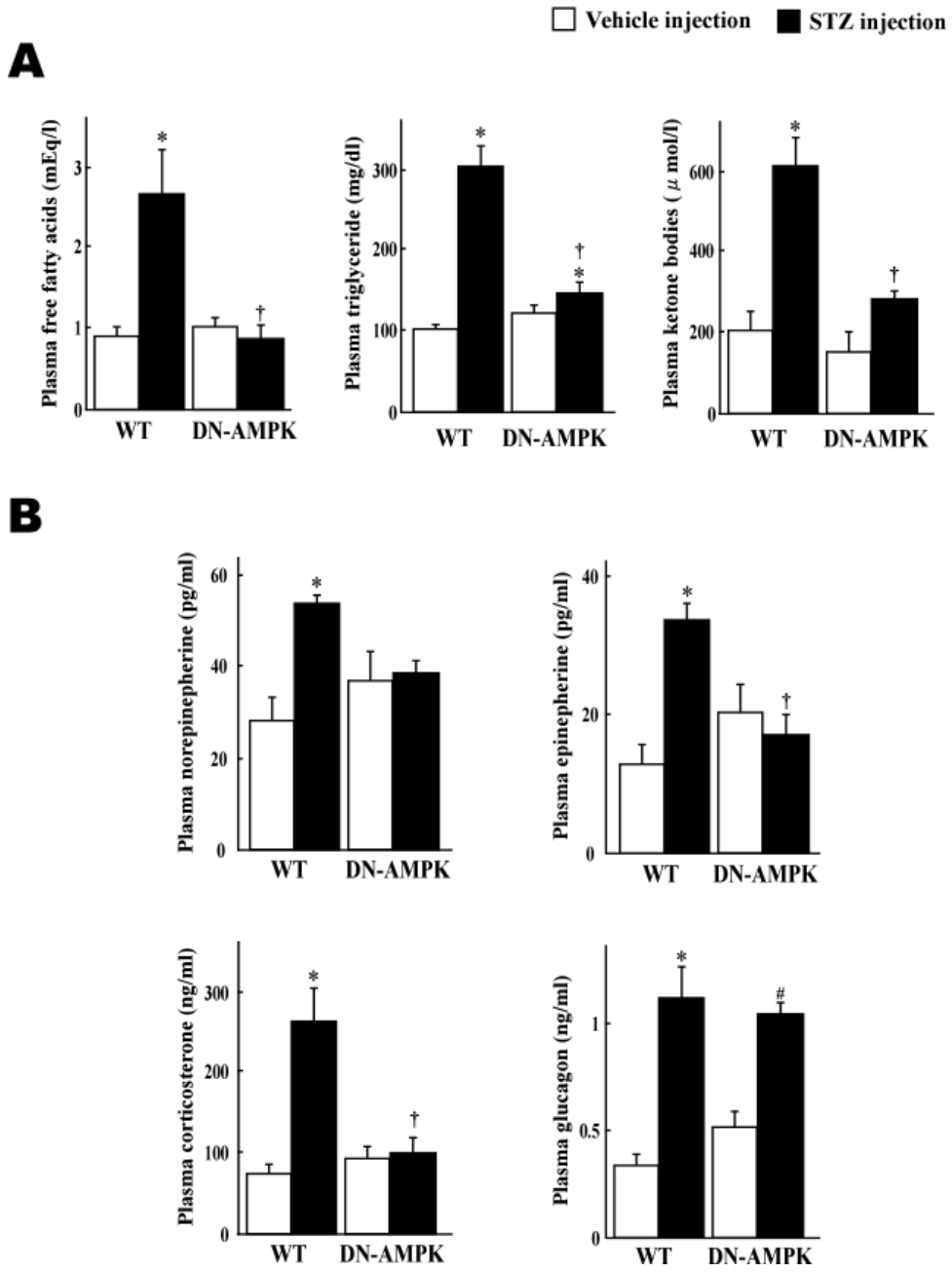


Figure 4. DN-AMPK mice improved plasma level of metabolites and gluconeogenic hormones, but not glucagon in STZ-induced IDDM.

(A) Concentrations of plasma free fatty acids, triglyceride and ketone bodies, and (B) concentrations of plasma norepinephrine, epinephrine, corticosterone and glucagon in WT and DN-AMPK mice 2 weeks after 1st injection of STZ or vehicle.

All quantitative data are mean \pm SEM. [n=7-10 in Fig. 4A and 4B, n=4 for plasma norepinephrine and epinephrine] Error bar represents the SEM. * p <0.05 versus vehicle-treated WT mice. † p <0.05 versus STZ-treated WT mice. # p <0.05 versus vehicle-treated DN-AMPK mice.

Fig. 5

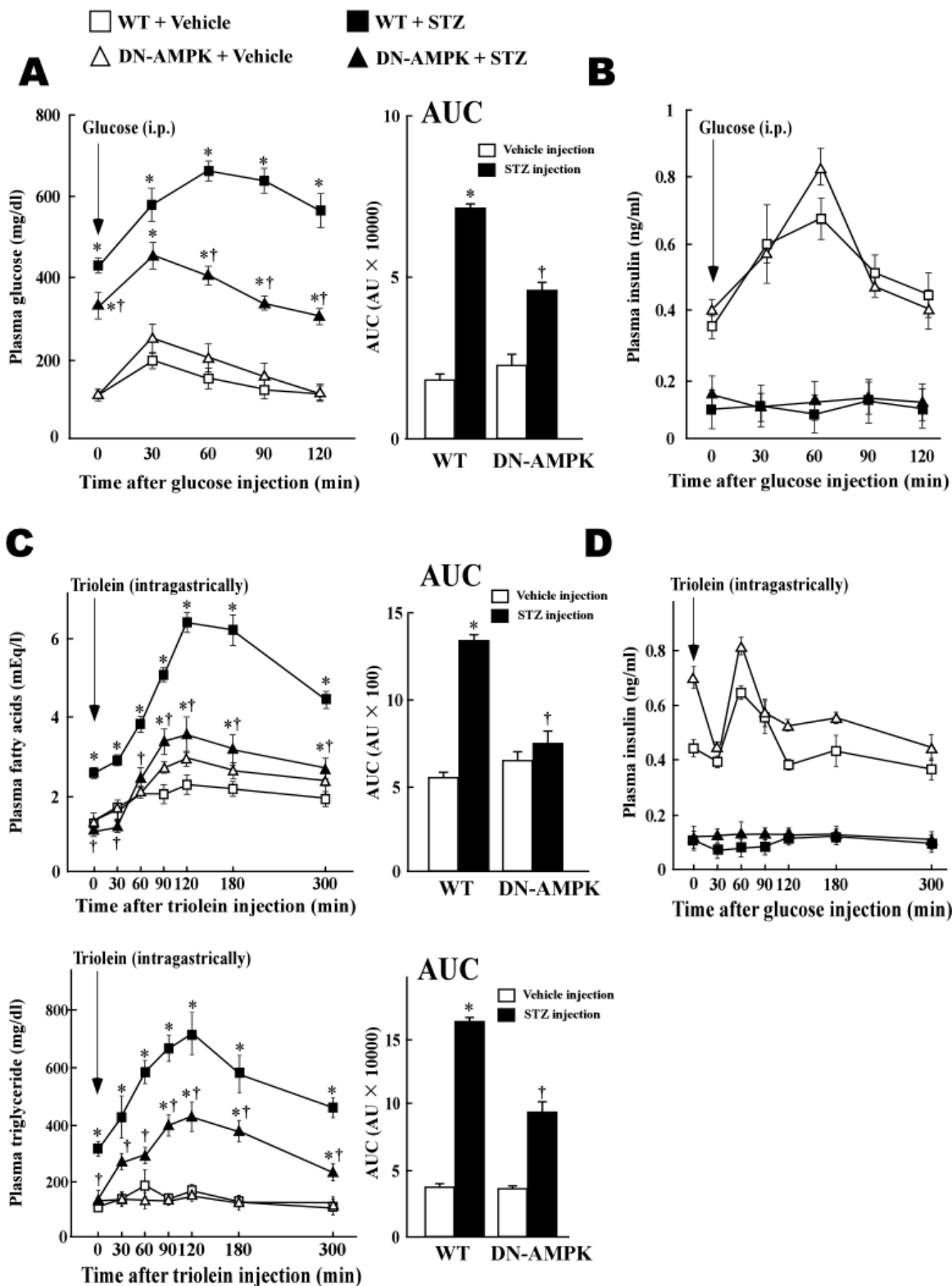
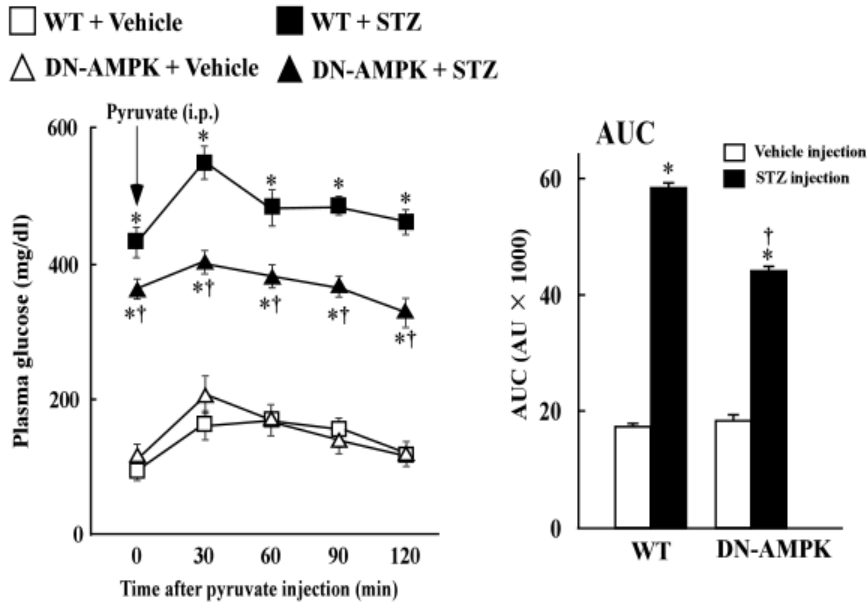


Fig. 5

E



F

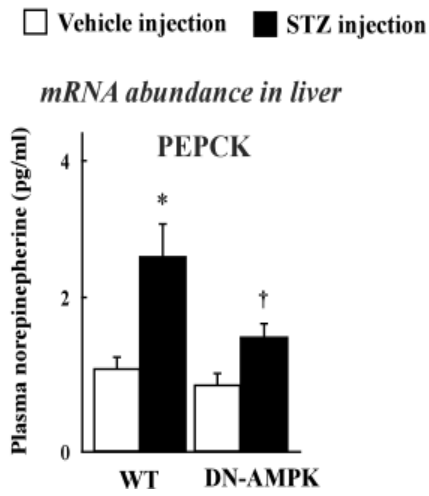


Figure 5. DN-AMPK mice improved systemic glucose and lipid metabolism in STZ-induced IDDM.

(A, B) Plasma concentrations of glucose (A) and insulin (B) during intraperitoneal (i.p.) glucose injection 1 week after 1st injection of STZ or vehicle.

(C, D) Plasma concentrations of free fatty acids and triglyceride (C) and insulin (D) during fat loading test 1 week after 1st injection of STZ. Triolein was ingested intragastrically by gavage.

(E) Plasma concentration of glucose during intraperitoneal (i.p.) pyruvate tolerance test 1 week after 1st injection of STZ or vehicle, and mRNA abundance of PEPCK in the liver 2 week after the injection.

Bar graphs: area under the curve (AUC) of plasma glucose concentration. AU, arbitrary unit. WT + vehicle: vehicle-treated WT mice; WT + STZ: STZ-treated WT mice; DN-AMPK + vehicle: vehicle-treated DN-AMPK mice; DN-AMPK + STZ: STZ-treated DN-AMPK mice.

(F) mRNA abundance of PEPCK in liver in WT and DN-AMPK mice 2 weeks after 1st injection of STZ or vehicle.

All quantitative data are mean \pm SEM [n=6 for (A-D), n=4 for (E), n=6-8 for (F)]. Error bar represents the SEM. * $p < 0.05$ versus vehicle-treated WT mice. † $p < 0.05$ versus STZ-treated WT mice.

Fig. 6

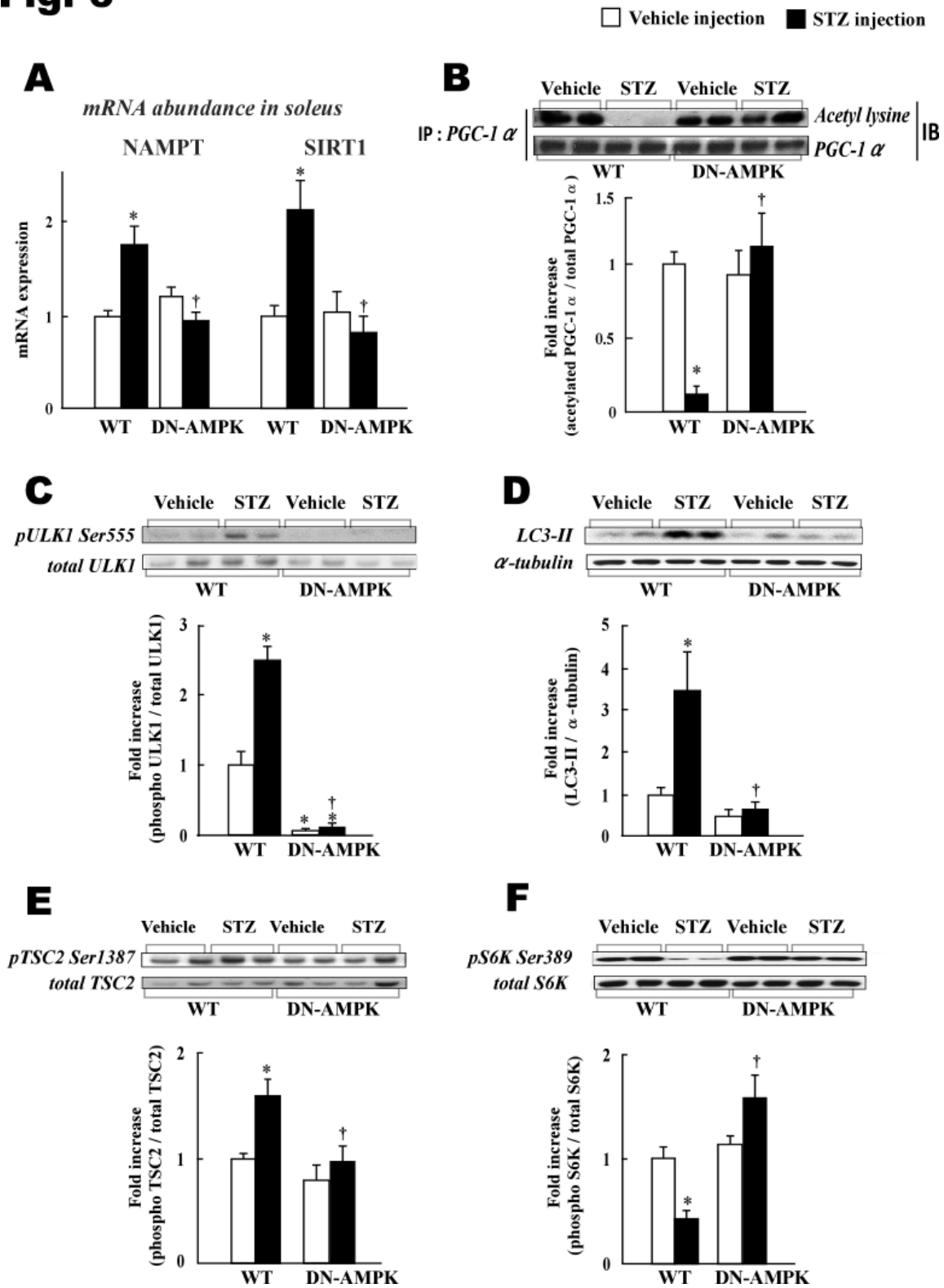


Figure 6. Down-stream signals of AMPK in soleus muscle in WT and DN-AMPK mice after injection of STZ or vehicle.

(A) mRNA abundance of NAMPT and SIRT1 in soleus muscle, (B) protein abundance of acetylated PGC-1 α in red portion of gastrocnemius muscle, (C) phosphorylation (Ser555) of ULK1 in soleus muscle, (D) protein abundance of LC3-II in soleus muscle, (E) phosphorylation (Ser1387) of TSC2 in soleus muscle, and (F) phosphorylation (Ser389) of S6K in soleus muscle, in WT and DN-AMPK mice 2 weeks after 1st injection of STZ or vehicle.

Data of bar graphs were expressed as percentage of total PGC-1 α (B), total ULK1 (C), α -tubulin (D), total TSC2 (E) and total S6K (F), respectively. All quantitative data are mean \pm SEM. (n=5-10) Error bar represents the SEM. * p <0.05 versus vehicle-treated WT mice. $\dagger p$ <0.05 versus STZ-treated WT mice.

Fig. 7

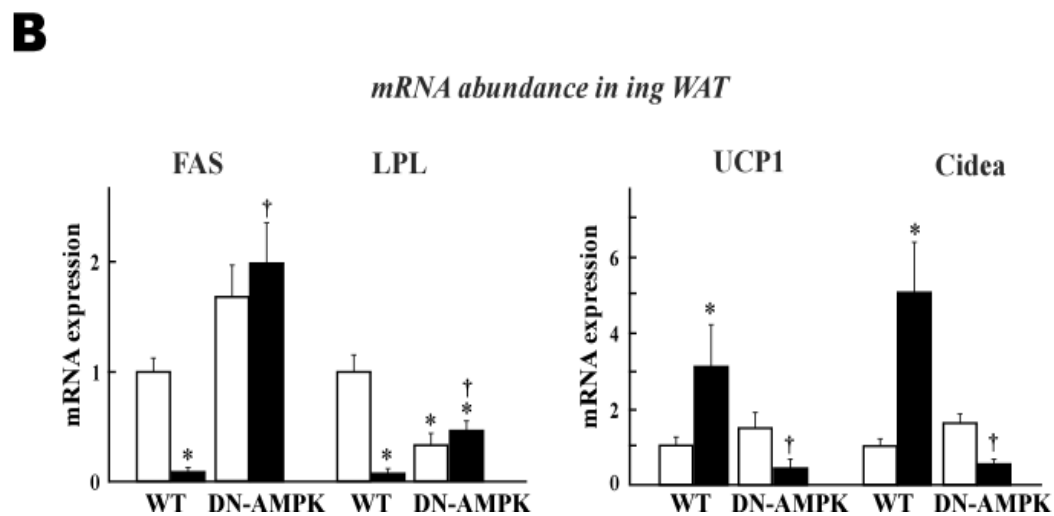
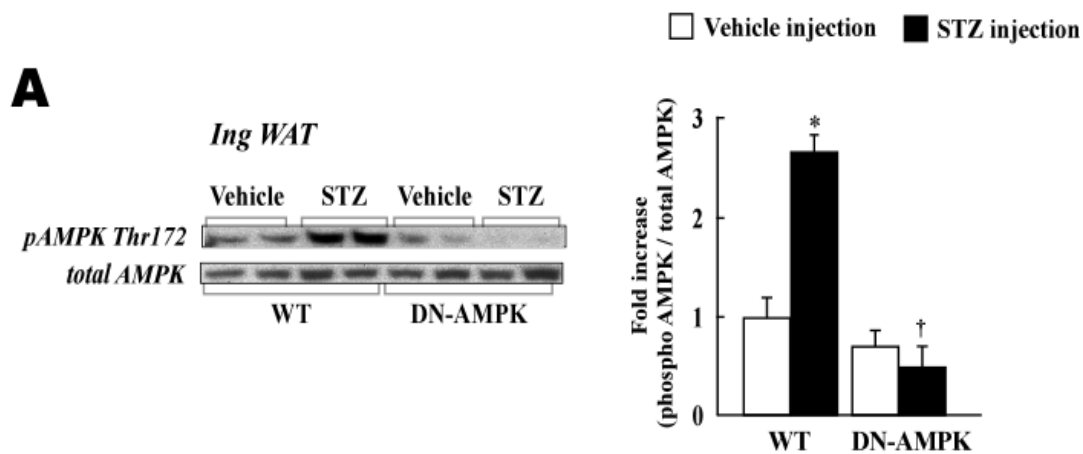


Figure 7. DN-AMPK mice suppressed AMPK activation and recovered altered gene expressions in WAT in STZ-induced IDDM.

(A) Representative immunoblot of phosphorylation (Thr172) and total AMPK ($\alpha 1$ plus $\alpha 2$) in inguinal (Ing) WAT in WT and DN-AMPK mice 2 weeks after 1st injection of STZ or vehicle. The Bar graph at right side shows the quantitative data expressed as percentage of total AMPK ($\alpha 1$ plus $\alpha 2$).

(B) mRNA abundance of FAS, LPL, UCP1 and Cidea in inguinal WAT in WT and DN-AMPK mice 2 weeks after 1st injection of STZ or vehicle.

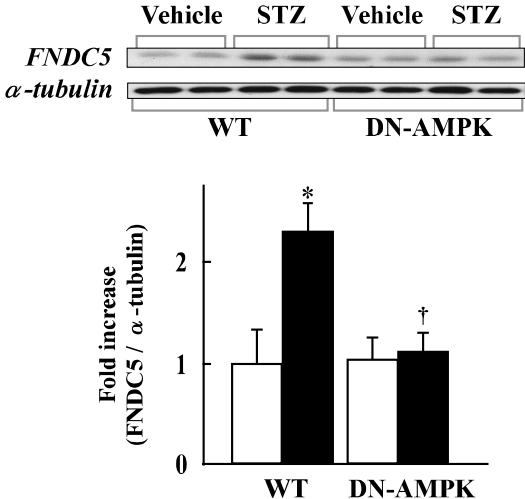
All quantitative data are mean \pm SEM. [n=4 for (A) and n=6 for (B)] Error bar represents the SEM.

* $p < 0.05$ versus vehicle-treated WT mice. † $p < 0.05$ versus STZ-treated WT mice.

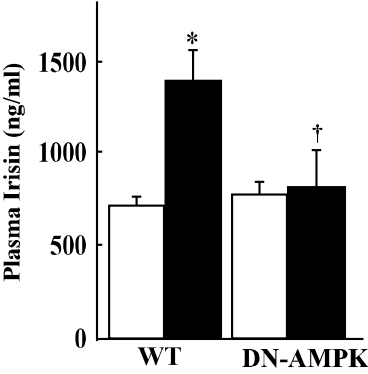
Fig. 8

□ Vehicle injection ■ STZ injection

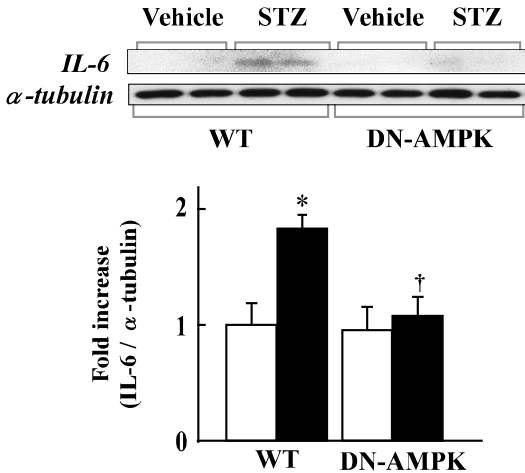
A



B



C



D

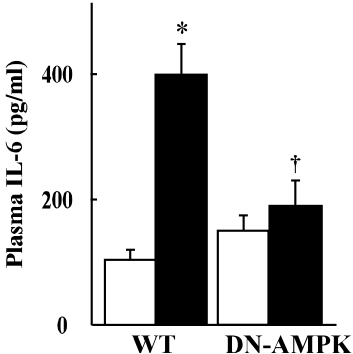


Figure 8. STZ-induced IDDM increased expression of myokines irisin and IL-6 in skeletal muscle in AMPK-dependent manner.

(A) Protein abundance of FNDC5, the precursor of irisin, in soleus muscle, (B) plasma concentration of irisin, (C) protein abundance of IL-6, and (D) plasma concentration of IL-6, in WT and DN-AMPK mice 2 weeks after 1st injection of STZ or vehicle. Data of bar graph for immunoblots were expressed as percentage of that of α -tubulin. Representative immunoblots with antibodies are shown above the quantitative data.

All quantitative data are mean \pm SEM (n=5-6). Error bar represents the SEM. * p <0.05 versus vehicle-treated WT mice. † p <0.05 versus STZ-treated WT mice.

Fig. 9

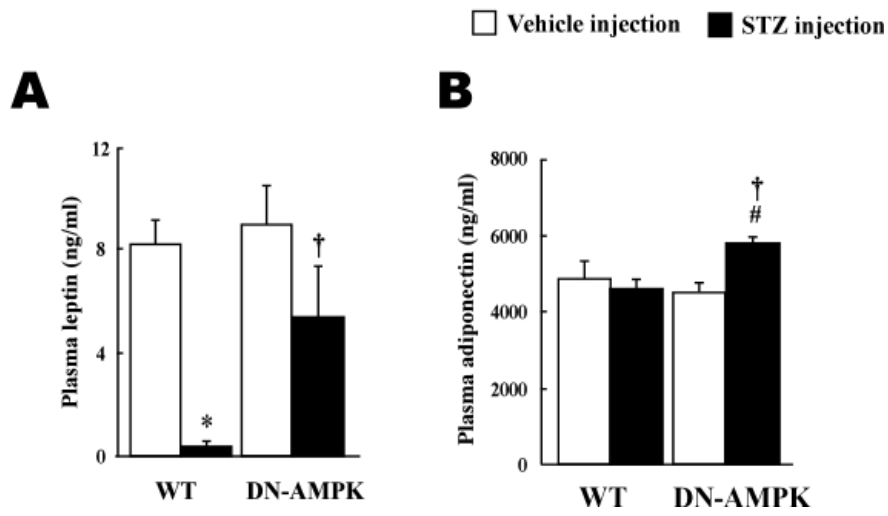


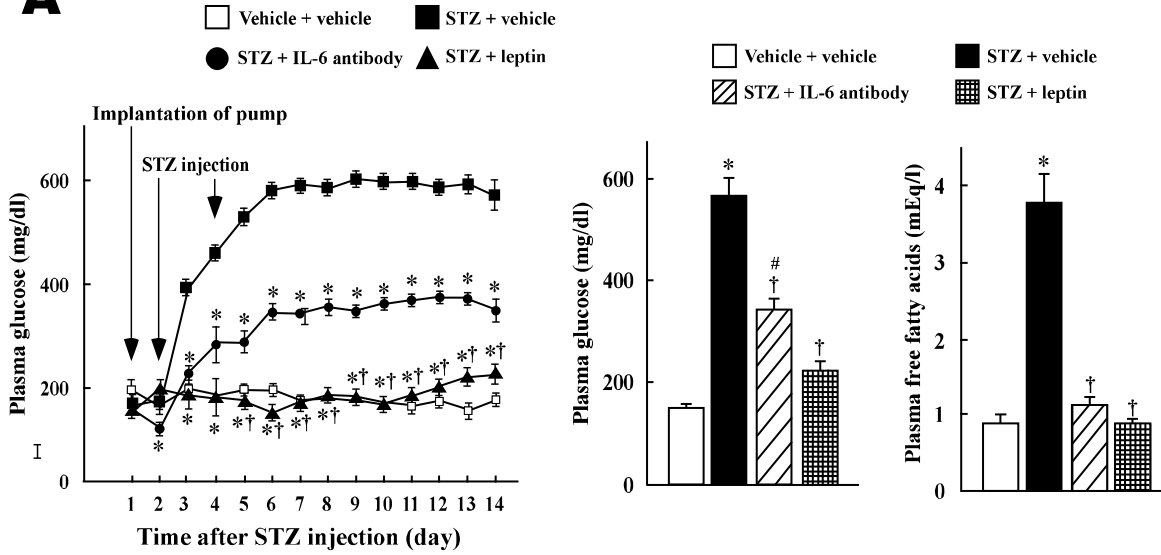
Figure 9. DN-AMPK mice altered plasma leptin and adiponectin levels in STZ-induced IDDM.

(A, B) Plasma concentrations of (A) leptin and (B) high molecular weight of adiponectin in WT and DN-AMPK mice 2 weeks after 1st injection of STZ or vehicle.

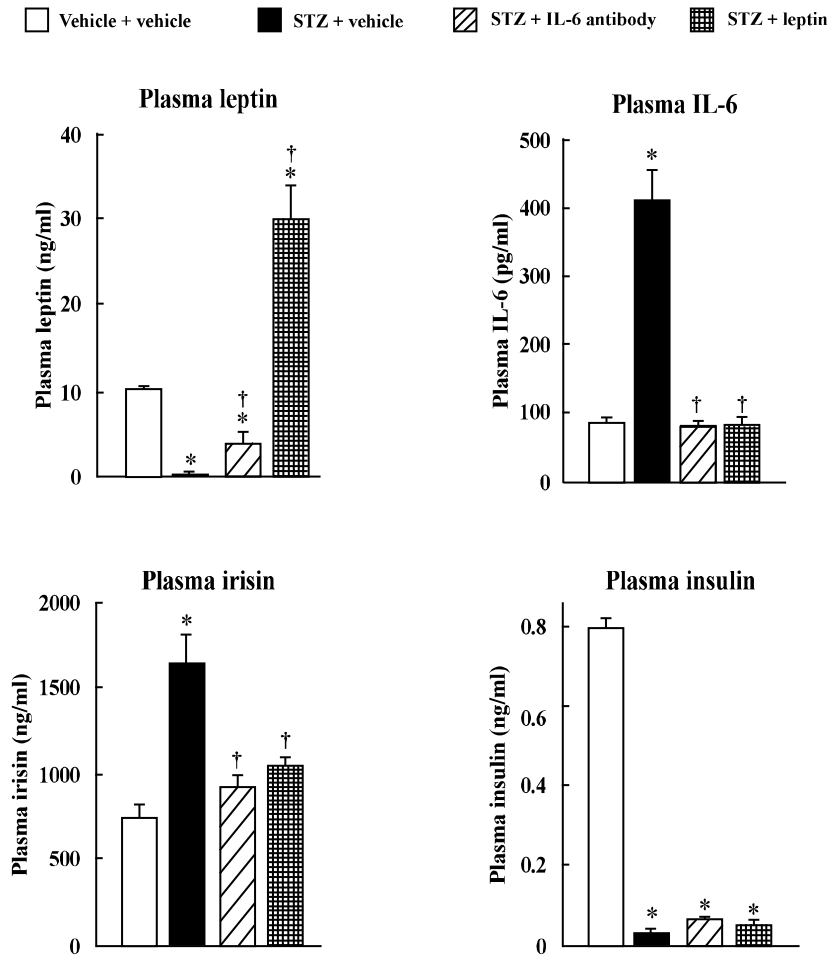
All quantitative data are mean \pm SEM (n=7-9). Error bar represents the SEM. * p <0.05 versus vehicle-treated WT mice. † p <0.05 versus STZ-treated WT mice. # p <0.05 versus vehicle-treated DN-AMPK mice.

Fig. 10

A



B



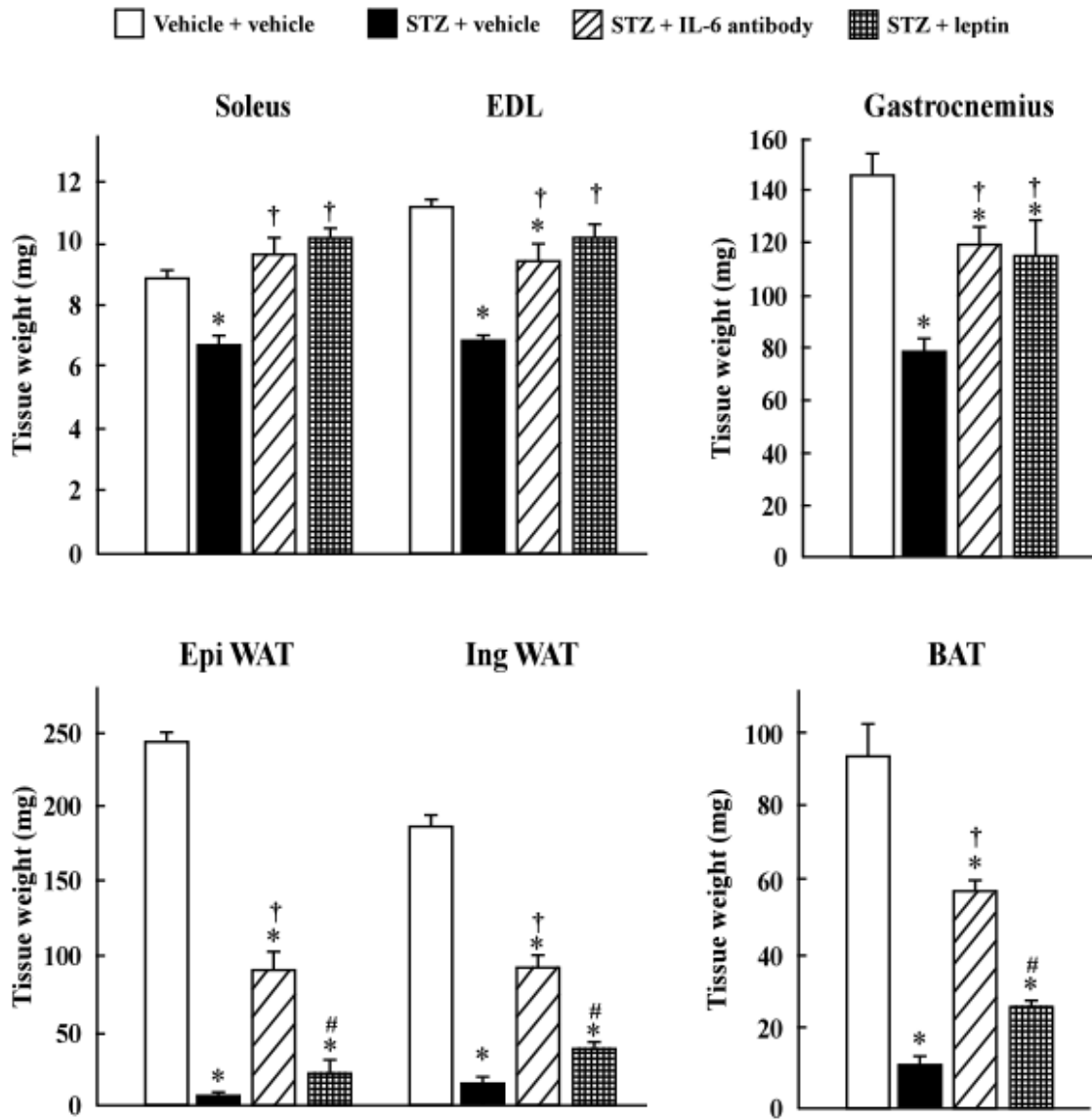
C

Figure 10. Chronic infusion of leptin or neutral antibody for IL-6 improved metabolic abnormalities in STZ-induced IDDM.

(A) Changes in plasma glucose concentration in vehicle- and leptin-treated and IL-6 antibody-treated C57BL/6J mice after STZ injection. Osmotic minipump was implanted s.c. on 1st day of the experiment, and STZ was injected twice on the 2nd and 4th day.

Left graph: changes in plasma glucose concentration for 2 weeks. Vehicle + vehicle: vehicle-treated and vehicle infused mice; STZ + vehicle: STZ-treated and vehicle-infused mice; STZ + IL-6 antibody: STZ-treated and IL-6 antibody-infused mice; STZ + leptin: STZ-injected and leptin-infused mice. * $p < 0.05$ versus STZ-treated and vehicle-infused mice.

Middle and Right graphs: concentrations of glucose (middle) and free fatty acids (right) at 2 weeks after implantation of pump and STZ injection. Vehicle + vehicle: vehicle-treated and vehicle infused mice; STZ + vehicle: STZ-treated and vehicle-infused mice; STZ + IL-6 antibody: STZ-treated and IL-6 antibody-infused mice; STZ + leptin: STZ-injected and leptin-infused mice. * $p < 0.05$ versus vehicle-infused and vehicle-treated (without STZ injection) mice.

(B) Concentrations of plasma leptin, IL-6, irisin and insulin in vehicle- and leptin-treated and IL-6 antibody-treated C57BL/6J mice at 2 weeks after implantation of pump and STZ injection. * $p < 0.05$

versus corresponding value on the 1st day. † $p < 0.05$ versus corresponding value in vehicle-infused and STZ-treated mice.

(C) Tissue weights of soleus, EDL, gastrocnemius, Epi and Ing WAT and BAT 2 weeks after implantation of pump and STZ injection. * $p < 0.05$ versus vehicle-infused and vehicle-treated (without STZ injection) mice. † $p < 0.05$ versus vehicle-infused and STZ-treated mice. # $p < 0.05$ versus IL-6 antibody-infused and STZ-treated mice.

All quantitative data are mean \pm SEM (n=4). Error bar represents the SEM.

Fig. 11

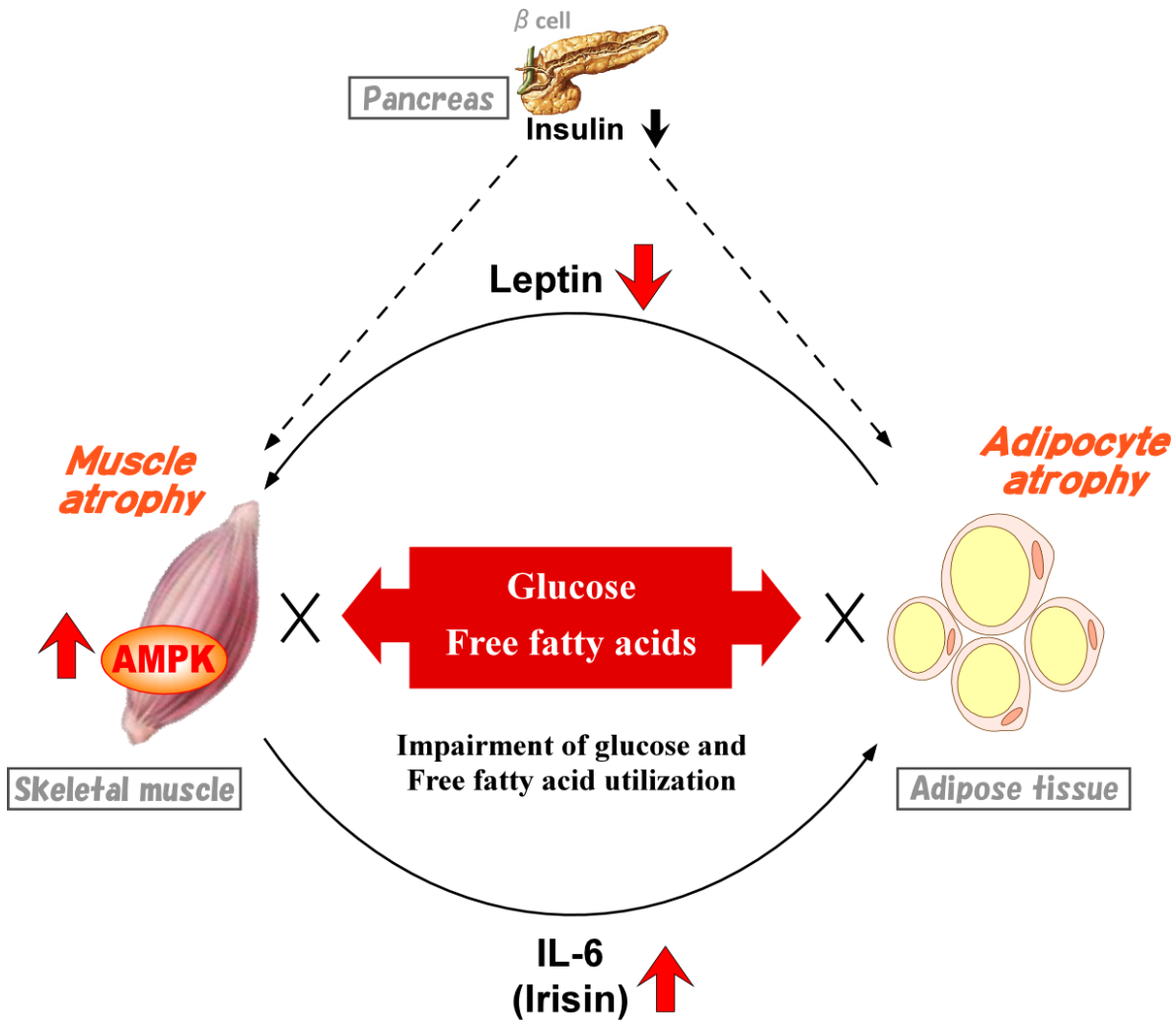


Figure 11. Vicious cycle in organ networks causes metabolic abnormalities in STZ-induced IDDM. STZ-induced IDDM activates AMPK in skeletal muscles, induces muscle atrophy, and increases plasma levels of IL-6 and irisin. IL-6 and/or irisin simulate UCP1 expression and lipolysis in adipose tissue, which cause atrophy of adipose tissue and decrease of plasma leptin level. Decreased plasma leptin level suppresses glucose and lipid utilization in skeletal muscle, and further induces muscle atrophy. Decreased plasma level of leptin as well as insulin also increases glucose production in the liver. Inhibition of AMPK activity in skeletal muscle improves metabolic abnormalities and tissue and body weight loss in IDDM, reducing plasma levels of IL-6 and irisin, and increasing plasma levels leptin and adiponectin. Chronic infusion of leptin or neutral antibody of IL-6 improves metabolic abnormalities and tissue weight loss in IDDM, similar to those in muscle-specific DN-AMPK expressing mice.

Table 1. List of kits for measurement of blood metabolites and hormones

Plasma	Product name	Catalog No.	Company
Glucose	Glucose CII-test	439-90901	Wako, Osaka, Japan
Free fatty acids	NEFA C-test	279-75401	Wako, Osaka, Japan
Triglyceride	Triglyceride E-test	432-40201	Wako, Osaka, Japan
Ketone bodies	Whole ketone bodies kit	AK-5601, AK-5602	Kinos, Tokyo, Japan
Insulin	Mouse Insulin ELISA KIT (U-type)	AKRIN-031	Shibayagi, Gunma, Japan
Glucagon	Glucagon EIA	YK090	Yanaihara Institute Inc., Shizuoka, Japan
Corticosterone	Corticosterone EIA	YK240	Yanaihara Institute Inc., Shizuoka, Japan
IL-6	Mouse IL-6 Assay Kit	27768	Immuno-Biological laboratories, Gunma, Japan
Irisin	Irisin/FNDC5 (16-127), Human/Mouse/Rat, ELISA kit	EK-067-16	Phoenix Pharmaceuticals, Inc., Burlingame, CA
Leptin	mouse leptin ELISA kit	EZML-82K	Milipore, Missouri, USA
Adiponectin	Mouse/Rat High Molecular Weight Adiponectin ELISA KIT	AKMAN-011	Shibayagi, Gunma, Japan

Table 2. List of antibodies

Antibody name	Catalog No.	Company name	Dilution
phospho AMPK α (Thr172)	2531	Cell Signaling Technology	1 to 1000
total AMPK α	2532	Cell Signaling Technology	1 to 1000
alpha 1	Affinity-purified antibody made originally (45)		1 to 10000
alpha 2	ab3760	Abcam	1 to 1000
phospho AKT (Ser473)	9271	Cell Signaling Technology	1 to 1000
total AKT	9272	Cell Signaling Technology	1 to 1000
Acetylated-Lysine Antibody	9441	Cell Signaling Technology	1 to 1000
PGC-1 (H-300)	sc-13067	Santa Cruz Biotechnology	1 to 1000
Phospho ULK1 (Ser555)	5869	Cell Signaling Technology	1 to 1000
total ULK1	A7481	Sigma	1 to 1000
LC3	2775	Cell Signaling Technology	1 to 1000
α -Tubulin	2144	Cell Signaling Technology	1 to 1000
Phospho TSC2 (Ser1387)	5584	Cell Signaling Technology	1 to 1000
Total TSC2	3612	Cell Signaling Technology	1 to 1000
Phospho mTOR (Ser2448)	2971	Cell Signaling Technology	1 to 1000
Total mTOR	2972	Cell Signaling Technology	1 to 1000
Phospho S6K (Thr389)	9205	Cell Signaling Technology	1 to 1000
Total S6K	9202	Cell Signaling Technology	1 to 1000
FNDC5	ab93373	Abcam	1 to 50
IL-6	ab6672	Abcam	1 to 1000

Cell Signaling Technology, Danvers, MA, USA

Abcam, Boston MA, USA

Santa Cruz Biotechnology, California, USA

Sigma, Tokyo, Japan

Table 3. List of primers for quantitative real-time PCR

Primer name	Forward primer sequence	Reverse primer sequence
Nampt	CCGCCACAGTATCTGTTCTT	AGTGGCCACAAATTCCAGAGA
SIRT1	GGCCCTTGTAACAACAAAATAC	GGCAACAAGAGCTGACAGTAAAT
PEPCK	GGTGTTTACTGGGAAGGCATC	CAATAATGGGGCACTGGCTG
Acidic ribosomal protein	AGATTCGGGATATGCTGTTGG	AAAGCCTGGAAGAAGGAGGTC
UCP1	GGCCCTTGTAACAACAAAATAC	GGCAACAAGAGCTGACAGTAAAT
Cidea	TGCTCTTCTGTATCGCCCAGT	GCCGTGTTAAGGAATCTGCTG
FAS	TTGCTGGCACTACAGAATGC	AACAGCCTCAGAGCGACAAT
LPL	AGGGCTCTGCCTGAGTTGTA	AGAAATTTTGAAGGCCTGGT
36B4	GGCCCTGCACTCTCGCTTTC	TGCCAGGACGCGCTTGT